Assessment of thermal circulations in strike-slip fault systems: the Terme di Valdieri case (Italian western Alps)

A. Baietto, P. Cadoppi, G. Martinotti, P. Perello, P. Perrochet and F.-D. Vuataz

Geological Society, London, Special Publications 2008; v. 299; p. 317-339
doi:10.1144/SP299.19

Assessment of thermal circulations in strike–slip fault systems: the Terme di Valdieri case (Italian western Alps)

A. BAIETTO[1], P. CADOPPI[1,4], G. MARTINOTTI[1], P. PERELLO[2], P. PERROCHET[3] & F.-D. VUATAZ[5]

[1]*DST, Dipartimento di Scienze della Terra, Università di Torino, Via Valperga Caluso 35, 10125, Torino, Italy (e-mail: alessandro.baietto@unito.it)*

[2]*SEA Consulting Srl, Via Cernaia 27, 10121, Torino, Italy*

[3]*CHYN, Centre d'Hydrogéologie, Université de Neuchâtel, Rue Emile-Argand 11– CP 158 CH-2009 Neuchâtel, Switzerland*

[4]*CNR-IGG, Istituto di Geoscienze e Georisorse, Sezione di Torino, Via Valperga Caluso 35, 10125, Torino, Italy*

[5]*CREGE, Centre for Geothermal Research, c/o CHYN, Rue E.-Argand, CP 158, CH-2009 Neuchâtel, Switzerland*

Abstract: Individual faults, faults linking at depth in flower structure zones and jogs bounded by faults are common structural elements in strike–slip fault systems and can play an important role in controlling thermal fluid flows. This paper explores the influence of these structures on the thermal circulations and fluid outflows of Terme di Valdieri, in the crystalline basement of the Argentera Massif (western Alps). In this site, thermal waters upwell at the tip of a NW-trending right-lateral fault, but exactly which structures control infiltration of meteoric waters and deep circulation is not clear from field surveys. Three-dimensional thermohydraulic numerical models calculated in steady-state and in transient regimes are presented for three alternative hypotheses. These account for circulations occurring: (i) within a single fault and adjoining host rocks; (ii) in faults intersecting at depth; and (iii) in faults interacting by means of a permeable step-over. The simulations show that advective flows can coexist with convective flows in models (i) and (iii), provided that the fault permeabilities are higher than 2×10^{-13} m^2, while advection prevails in model (ii) at all values of permeability. Model (iii) achieves the best fit to the data under the assumption of advective and convective flows. This finding provides a first quantitative estimate of the importance of jog structures bounded by strike–slip faults in favouring thermal outflows. Moreover, the numerical results suggest that thermal convection can coexist with advection also in mountainous settings.

Faults profoundly affect the patterns and rates of fluid flow in present-day flow systems in the upper seismogenic crust (Yeamans 1983; Sibson 1987; Henley & Adams 1992; Hickman *et al.* 1995; Curewitz & Karson 1997; Benoit 1999). Fluids flowing within large faults control the mobilization, transport and deposition of chemical species and influence heat transfer through the crust (Cox *et al.* 2001; Jaboyedoff & Pastorelli 2003). The thermal effect of fault-related fluid circulations can account for the deposition of ores at anomalously shallow depths (Bethke & Marshak 1990; Garven *et al.* 1993) and the emergence of hot springs (Alföldi *et al.* 1985; Forster & Smith 1989). The quantitative assessment of the structural influence of fault zones on thermal flow systems requires an accurate conceptual model of fault zone structure coupled to data regarding the hydraulic properties (e.g., permeability, porosity and storativity) of both the fault zone and the adjacent rock masses (Evans *et al.* 1997; Barton *et al.* 1995; Caine *et al.* 1996; Parry 1998; Sibson 2001). However, these parameters are difficult to assess due to their spatial and temporal variability and the scarcity of direct measurements (Smith 1980; Sibson 1994).

In order to obtain insights into fault-related thermal flow systems, several researchers have applied hydrogeological numerical modelling to a range of tectonic contexts, for example to extensional sedimentary basins (López & Smith 1995; Wisian & Blackwell 2004; McKenna & Blackwell 2004), to accretionary wedges (Henry 2000; Cutillo *et al.* 2003), and to oceanic spreading centres (Fehn & Cathles 1979; Travis *et al.* 1991). In general, these models aim to determine the conditions allowing high surface heat flows and high temperatures both in reservoirs and at

From: WIBBERLEY, C. A. J., KURZ, W., IMBER, J., HOLDSWORTH, R. E. & COLLETTINI, C. (eds) *The Internal Structure of Fault Zones: Implications for Mechanical and Fluid-Flow Properties*. **299**, 317–339.
DOI: 10.1144/SP299.19 0305-8719/08/$15.00

springs as a function of the structural and hydraulic properties attributed to fault zones and hosting rocks. Despite the common association between strike–slip faults and hydrothermal systems (Sibson 1987; Henley & Adams 1992), quantitative documentation of fluid and heat flow patterns in these tectonic contexts has received relatively little attention (Kasameyer *et al.* 1984).

It is uncertain what controls are exerted on thermal circulations by structures that commonly occur in contexts of wrench tectonics (e.g., single fault strands, coalescing faults, step-over faults). This is an important aspect of the problem because there is evidence that active outflow sites and preserved hydrothermal deposits are most commonly located at the terminations of individual faults and where multiple faults interact (Sibson 1987; Curewitz & Karson 1997). Moreover, while numerical simulation applied to sedimentary basins has contributed to the recognition of thermal processes driven by both advective and convective flows (López & Smith 1995, 1996; Garven *et al.* 2001; Simms & Garven 2004; Thornton & Wilson 2007), this remains to be verified in strike–slip fault-related thermal systems developed in basement rocks.

This study refers to a thermal outflow site located in the Argentera Massif (western Italian–French Alps), where several groups of hot springs, with temperatures of 30–70 °C and flow rates of 2–50 kg s^{-1}, emerge along regional NW–SE strike–slip faults (Fig. 1; Perello *et al.* 2001; Baietto 2007). As in all the other geothermal systems of the Alps (e.g., Vuataz 1982; Rybach 1995; Perello 1997; Martinotti *et al.* 1999; Pastorelli *et al.* 1999, 2001; Marini *et al.* 2000),

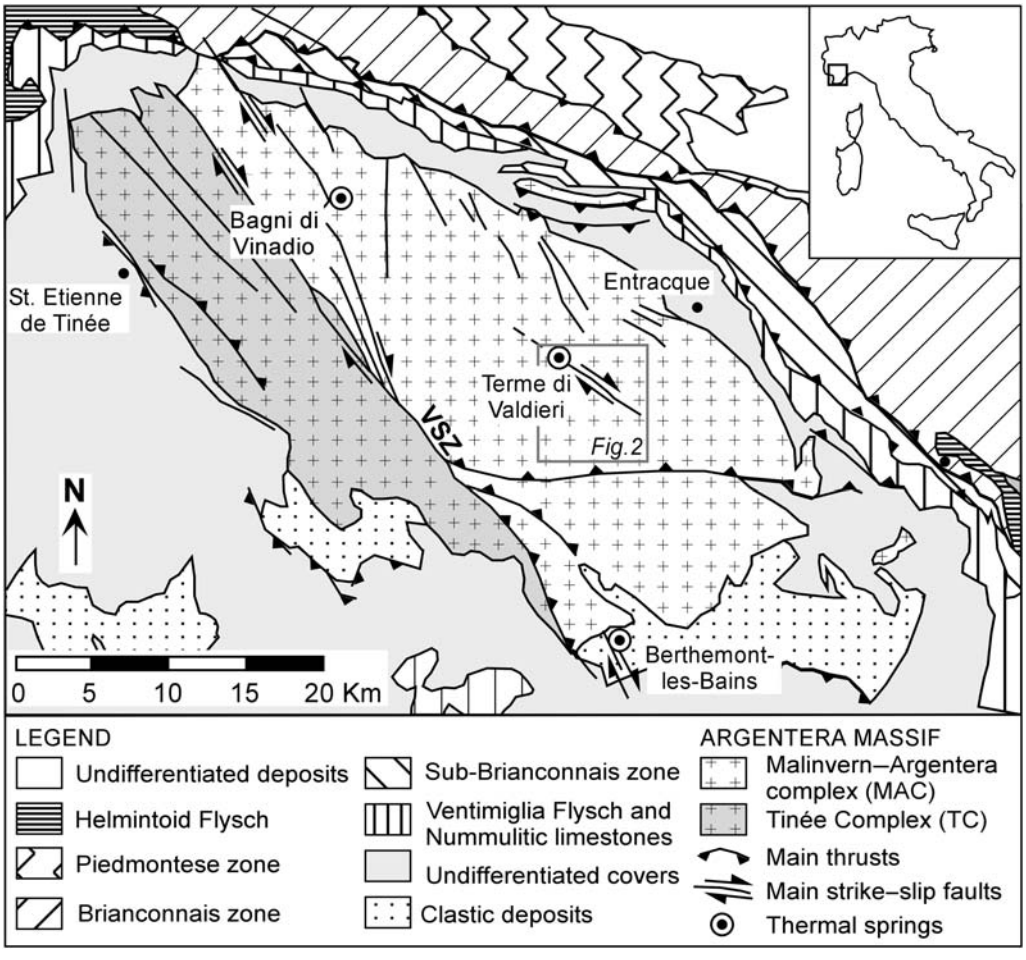

Fig. 1. Sketch map of the Argentera Massif and adjoining regions. VSZ, Valletta Shear Zone. Groups of thermal springs are located at the margins of NW–SE strike–slip faults at Bagni di Vinadio (I), Terme di Valdieri (I) and Berthemont-Les-Bains (F), exhibiting maximum outlet temperatures of 60, 70 and 30 °C, respectively.

the Argentera thermal discharges originate from the circulation at depth of meteoric waters that heat up and rapidly upwell to surface, in a region where active cooling of igneous bodies is absent. One of the most interesting among the Argentera thermal sites is represented by the Terme di Valdieri springs, a group of hot-water springs that discharge at the tip of a main strike–slip fault zone called the Lorusa Fault (Figs 1 & 2). Structural surveys have pointed out that the Lorusa Fault forms a channel which permits the final upwelling of the hot waters. However, the routes facilitating the penetration of cold water into the system and the nature of their circulation patterns remain unknown. In particular, it is not clear whether the Lorusa Fault acts as a unique pathway where fluids infiltrate, circulate while exchanging heat with rocks and upwell to the surface, or whether the circulation is partitioned among several strike–slip faults that are hydraulically connected through intersecting strands or through a permeable step-over. The purpose of this paper is therefore to explore the mechanisms of heat and fluid transport through the Valdieri faults using thermohydraulic numerical modelling in which some of the geometrical complexity related to strike–slip fault systems is taken into account. Sets of 3D numerical simulations of heat and fluid transport were carried out in steady-state and transient regimes to examine and compare the responses of the hot spring parameters as a function of the structural configuration and hydraulic properties attributed to the Valdieri faults and surrounding host rocks. These simulations yield insights into the conditions favouring the coexistence of advective flows governed by topographic gradients and convective flows driven by fluid density gradients in a strike–slip setting. Given the Alpine setting of the study area, the mechanisms governing water and heat transport along faults and the thermal state of the upper crust are also of strategic importance in both geothermal energy exploration and development and in the forecasting of risk related to underground engineering projects (e.g., deep tunnels).

Structural and hydrogeological setting of the Valdieri sector

The Argentera Massif (AM), the southernmost of the Alpine external massifs (others being Aar-Gothard, Aiguilles Rouges, Mount Blanc, Belledonne, Grandes Rousses and Pelvoux), is a slice of the European plate crystalline basement which crops out owing to its uplift and to the subsequent erosion of the overlying Mesozoic sedimentary succession (Helvetic–Dauphinois cover, HDC; Fig. 1). This massif represents one of the zones of the Western Alps with the highest concentration of thermal discharges. The main AM springs are located at Bagni di Vinadio (I), Terme di Valdieri (I), and Berthemont-Les-Bains (F; Fig. 1), exhibiting maximum outlet temperatures of 70, 60 and 30 °C respectively. The massif consists mainly of two gneissic complexes: to the east, the Malinvern–Argentera Complex (MAC), and to the west, the Tinée Complex (TC; Fig. 1). They are separated by a steep NW–SE striking mylonitic belt known as the Valletta Shear Zone (VSZ; Faure-Muret 1955; Bogdanoff 1986). This pre-Alpine structural element was reactivated by both ductile and brittle deformation during the Alpine Orogeny (Fry 1989). The TC is similar to the MAC in that it consists mainly of migmatitic gneisses related to pre-Alpine, high-grade metamorphism (Malaroda *et al.* 1970; Bogdanoff 1986). Fission-track analyses (Bigot-Cormier *et al.* 2000) reveal differential uplifts of the MAC and TC blocks. In the last 3.5 Ma, the MAC was characterized by a faster exhumation than the TC, with apparent uplift rates of *c.* 1.3 mm a^{-1}. According to Tricart (2004), the recent uplift of the AM results from the onset of a transpressive tectonic regime with dextral wrench faulting along the southern branch of the Alpine arc, close to the internal–external arc boundary.

In the area surrounding Terme di Valdieri, which forms part of the MAC, the main rock types are igneous rocks and migmatitic gneisses, the former consisting of medium- to coarse-grained granites and leucocratic aplites, and the latter, biotite-rich embrechites and leucocratic anatexites (Fig. 2a). The migmatitic gneisses outcrop mainly in the northern part of the mapped sector, whereas in the southern part, granite is prevalent. Close to the Terme di Valdieri site, the migmatitic gneisses crop out and overlie the granites at shallow depths. A main system of NW–SE strike–slip faults of Alpine age showing en-echelon geometries and evidence of right-lateral displacement cut pervasively through the migmatitic gneisses and granites in the area surrounding Valdieri (Perello *et al.* 2001). Subsidiary ENE–WSW striking faults characterized by left-lateral movements are associated with the main system. The springs of Terme di Valdieri discharge alongside the river bed of the Valletta Valley (Fig. 2a) next to the northwestern tip of a kilometre-scale NW–SE fault zone, the Lorusa Fault. Close to the thermal outlets, rock alterations and sulfide mineral deposits associated with the Lorusa Fault zone attest to the presence of earlier hydrothermal activity (Perello *et al.* 2001).

South of the Lorusa Fault, other kilometre-scale, NW-trending faults cross-cutting the Terme di Valdieri sector include the Cougne Fault, the S. Giovanni Fault, and the Valcuca Fault (cf. Fig. 2). Because their dips vary from SW to NE, these faults define an overall upward diverging

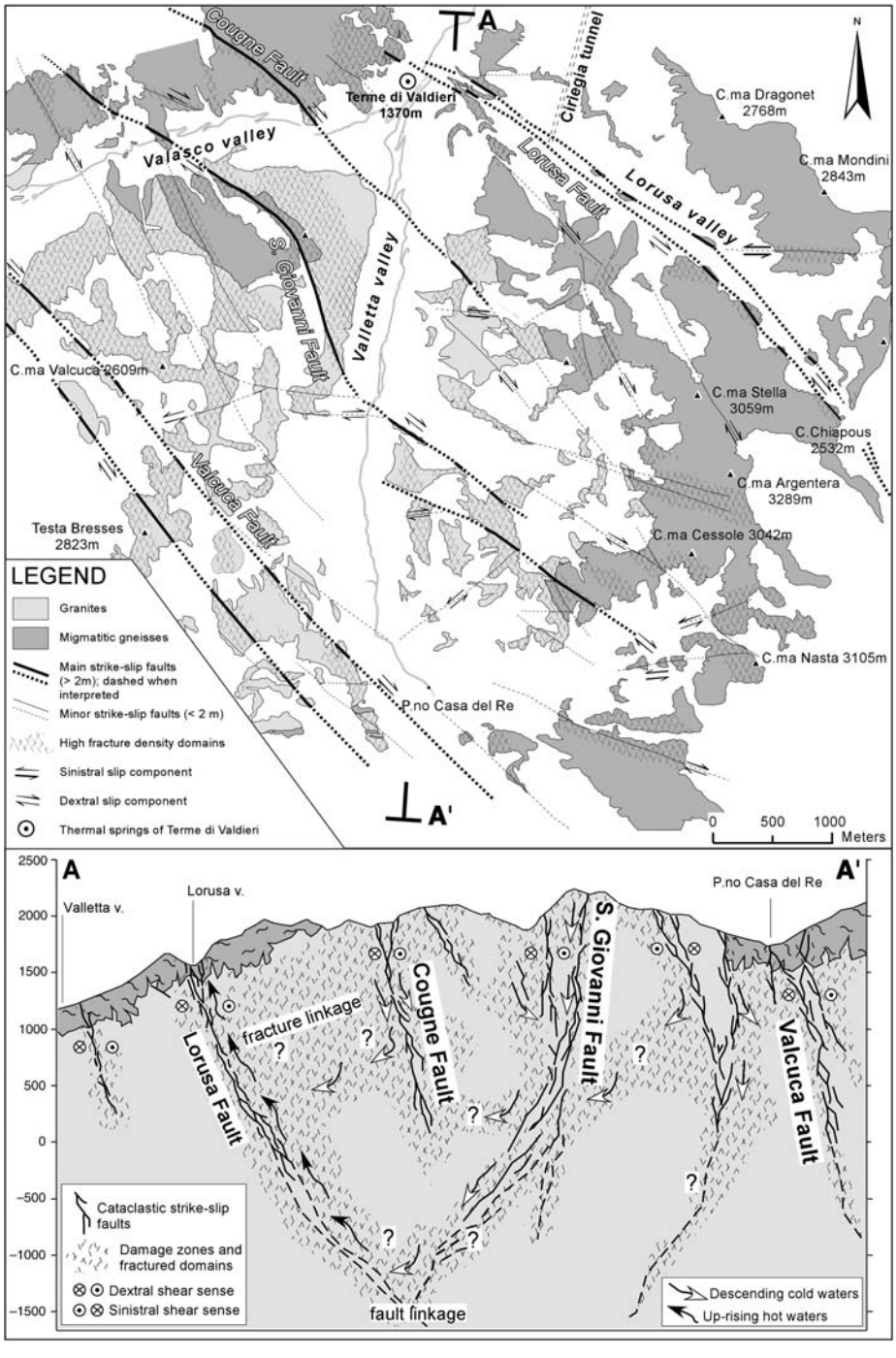

Fig. 2. Structural map (upper part, **a**) of the area surrounding the Terme di Valdieri springs. This area is pervasively cut by NW–SE strike–slip faults with right-lateral slip components and by subsidiary ENE–WSW striking faults with left-lateral slip. The Valdieri springs emerge through the damage zone at the northwestern tip of the Lorusa fault, a 7 km long NW–SE strike–slip fault characterized by a cataclastic core and fractured damage zones. A cross-section (lower part, **b**) along the A–A′ trace shows possible patterns of hydrothermal circulation. The occurrence of fault and fracture linkages can influence the descent of cold waters and the upwelling of hot waters.

geometry. Kinematic evidence associated with these faults indicates that this sector can be interpreted as a flower structure that developed in a context of right-lateral transpressive displacement (Baietto 2007). The faults probably converge at depth into a single shear zone, as suggested by existing flower structure models (Woodcock & Fischer 1986).

As for the Valdieri hot springs, it seems that an important role in hot-water outflow could be played by the particular geometrical configuration defined by the Lorusa and Cougne faults. The tip-line of the Lorusa Fault lies close (*c*. 2 km) to the inferred tip-line of the Cougne Fault. At the local scale, these two structures define a right-contractional step which corresponds to an area of intense fracturing which coincides with the thermal discharges of Valdieri.

As a consequence of different concentrations of oriented phyllosilicates, brittle deformation associated with the faults in the migmatitic gneisses and in the granites resulted in different fault architectures. The structure of the strike–slip faults which developed within the migmatitic gneisses is characterized, moving from the inner to the outer part of the fault zone, by a narrow phyllonitic gouge zone (where most of the slip is accommodated), by an intermediate zone of foliated cataclasites, and by an outer domain of highly fractured rocks. The gouge, cataclasite and fractured zones have thicknesses, respectively, of 0.1–2, 0.5–5 and 1–10 m. In contrast, within the granites, brittle deformation is accommodated by several discrete shear planes composing a pervasive network of fractures broadly distributed over the mapped area (Fig. 2b). These planes, which are concentrated in domains hundreds of metres thick, have fracture spacings ranging from a few centimetres to a metre and an aperture of a few millimetres. At various spacings, these domains enclose NW–SE-trending metre-width cataclastic zones.

Conceptual models of thermal circulation

Conceptual models of the groundwater flow system were arrived at by studying the physical and chemical properties of the hot springs and the geometrical and hydraulic characteristics of the fault zones in the Terme di Valdieri sector. These models constituted the basis for constructing numerical models that were then tested against data and used to assess the possible hydrodynamic properties of the Terme di Valdieri system. The Valdieri springs have a maximum outlet temperature of 70 °C (Baietto 2007). Mass balance calculations performed on the water temperatures and flow rates of the Valletta River provided an estimate of the bulk thermal discharge of *c*. 50 kg s^{-1}. The thermal waters have pH values of 9 and salinities of 0.2–0.4 g l^{-1}. Analyses of stable isotopes indicate a pure meteoric origin and, according to geothermometric calculations, the meteoric waters equilibrated at temperatures between 90 and 150 °C with hydrothermal minerals (Perello 1997; Perello *et al.* 2001; Baietto 2007). A temperature of 150 °C corresponds to depths of 5–6 km, assuming a geothermal gradient of 30 or 25 °C km^{-1} respectively, which are typical for the western Alps (Jaboyedoff 1999).

The meteoric origin of the fluids and mountainous setting of the Argentera Massif suggest that the process driving the Valdieri thermal flow is primarily controlled by advective flow related to differences in topographic elevation. The Valdieri springs are located at 1370 m, while adjoining summits reach 3000 m and have a mean elevation of 2600 m. However, two other processes might potentially influence the bulk geothermal system: thermal convection and pressure-driven flow after faulting. Thermal convection is created by fluid density gradients associated with changes in temperature, salinity and pressure (Evans & Raffensperger 1992). In their numerical simulations, Forster & Smith (1989) and López & Smith (1995) investigated the role played by factors such as fault and host rock permeability, regional heat flux, fault length and depth, relief, and geometry of the water table in influencing advective as opposed to convective heat transfer regimes within faults in mountainous regions. Up to now, it has not been clear to what extent the thermal flow is governed by regional topographic gradients or by thermal convection along the strike of the Valdieri faults. Numerical modelling is therefore used here to highlight the conditions which can favour the occurrence of these processes.

Pressure-driven flow after faulting can also control the hydrodynamics of faulted systems (Neuzil 1995; Faulkner & Rutter 2001; Garven *et al.* 2001). This process may result from the combination of conditions leading to fluid overpressures (e.g., decrease of porosity or increase of fluid volume over time) and tectonic loads (Bredehoeft & Hanshaw 1968). Earthquakes and swarm activity can account for fluid redistribution in response to the local generation of overpressure through fault-fracture meshes, but the level of overpressure that can accumulate depends on the tectonic setting, the localized stress state, and the extent of inherited brittle architecture (Sibson & Scott 1998). In the present case, despite the fact that the Argentera Massif is located in one of the most seismically active parts of the Alpine range (Calais *et al.* 2000), the largest instrumental earthquakes recorded in recent years occurred along the northern

margin of the Ligurian basin, south of the massif ($M_L = 6.0$, 1989; $M_L = 4.5$, 1995; Ritz 1991; Courboulex *et al.* 1998). Within the Argentera Massif, the Valletta Shear Zone was proposed as the locus of two relevant earthquakes in 1938 ($M_L = 5.1$) and 1959 ($M_L = 5.3$; Ghafiri 1995), but the last 50 years have been characterized only by low-magnitude earthquakes ($M_L < 3$; RSNI database). Owing to the low intensity of recent seismicity affecting the Argentera Massif (Larroque *et al.* 2001), and to the fact that transient effects associated with fault rupture in the crystalline basement are thought to vanish rapidly (Phillips 1991), it is reasonable to exclude the hypothesis that mechanisms such as pressure-driven flow after faulting can substantially influence the hydrodynamic behaviour of the Valdieri thermal system. For these reasons, this process is not considered in the simulations.

The definition of the geometries and structural architectures of fault zones by means of detailed field investigations has not been able to resolve the thermal circulation in the Valdieri area. The scant hydrogeological data available for this area are consistent with a range of alternative hypotheses concerning fluid and heat flow patterns. In the final part of its pathway, the thermal flow is confined to the borders of the Lorusa Fault, located in the shallower part within the gneisses and in the deeper part within the granites (Fig. 2b). The core zone of this fault constitutes an impermeable barrier to cross-flow circulation, allowing upward fluid flow and discharge at the Terme di Valdieri site. At *c*. 1 km east and at an altitude of 100 m below the Valdieri hot springs, the Lorusa Fault is intersected by the Ciriegia exploration tunnel (Fig. 2a). At this point, the reported inflows were 20 kg s^{-1} at a temperature of 20 °C, which is indicative of an apparent geothermal gradient of 20 °C km^{-1} (Bortolami & Grasso 1969) that can be attributed to downflowing cold waters. Data relative to the tunnel compared with those of the thermal springs help to define a scenario in which the hot waters of Valdieri ascend vertically close to the tip of the Lorusa Fault and concentrate a hot anomaly in the neighbourhood of the spring discharges without affecting the rest of the zone. However, whether the final part of the thermal water flow is reasonably well constrained, where cold waters penetrate and circulate, remains unknown. A crucial factor not yet revealed by field surveys is the degree of hydraulic connectivity among the different faults. This uncertainty involves the possibility either that the Lorusa Fault crosscuts other fault zones at depth, or that regions of enhanced permeability connect the Lorusa Fault with other permeable fault zones. Based on field evidence, three main conceptual models involving different fluid flow patterns are proposed as alternative descriptions of the Terme di Valdieri circulation. These include a single conduit model (model 1), a fault intersection model (model 2) and a fault interaction model (model 3).

In model 1, the thermal flow is focused within the Lorusa Fault, which acts as a single permeable channel allowing infiltration of cold waters, circulation and upward migration of heated waters towards the surface. Depending on the relative permeability of the Lorusa Fault and host rocks, either the damage zone of the Lorusa Fault may constitute the region where most of the fluids circulate and where heat transfer processes occur, or the thermal flow may be pervasively distributed through permeable fracture networks within the granites surrounding the fault. In the latter case, fluids would infiltrate pervasively through fracture networks (fracture linkage; cf. Fig. 2b) developed within the granites and migrate in tortuous pathways towards the Lorusa Fault, where they would focus and emerge at the springs. In models 2 and 3, the thermal flow is partitioned between several conduits corresponding to the borders of main NW–SE striking faults. In this case (cf. Fig 2b), additional amounts of heated waters may be driven to the Lorusa Fault, either by the intersection of this structure with the S. Giovanni Fault, or by the interaction generated by the Lorusa Fault with the Cougne Fault. In model 2, the Lorusa and S. Giovanni Faults crosscut at depth and both constitute permeable channels where fluids infiltrate. Under the influence of pressure gradients, meteoric waters are driven at depth toward the Lorusa Fault and then up to the Terme di Valdieri springs. In model 3, it is assumed that the zone of intense fracturing observed between the Lorusa and Cougne Faults which corresponds to a contractional step constitutes a permeable bridge interconnecting the thermal circulations that occur within the two faults.

Methodology and boundary conditions of numerical models

The alternative hydrogeological hypotheses proposed for the Valdieri geothermal system were investigated using 3D thermo-hydraulic numerical simulations. These were carried out by integrating increasing degrees of geometrical complexity into a base model, thus finally allowing the different thermal flow hypotheses to be compared. The use of 3D rather than 2D modelling allowed the authors to account more fully for the lateral thermal effects of the geothermal system under study, thus providing a more realistic representation of the heat flow field through the area. The hypotheses concerning thermal flow were investigated

through the three discretization geometries illustrated in Fig. 3. These include a base model where only the Lorusa Fault is taken into account (model 1; Fig. 3a & b), a model where the Lorusa Fault is crosscut at depth by the S. Giovanni Fault (model 2; Fig. 3c), and a model where the Lorusa Fault is in hydraulic connection with the Cougne Fault through a permeable jog (model 3; Fig. 3d). The location of the hot springs is shown in Figure 3a. In the base discretization geometry, the Lorusa Fault is represented by a vertical slab 200 m wide and 7 km long, which is enclosed within a block of host rocks 9.4 km long and 5 km wide. The length of this model was fixed to the SE by the southern tip of the fault and to the NW by the mountain ridge, while its width was varied according to the hypothesis under test. In model 1, the width is 5 km and is constrained to the NE by the Cougne Fault, which in this case is considered as not contributing to the active thermal flow. In model 2, the width is 7.5 km and the NE limit corresponds to the outer border of the S. Giovanni fault. In model 3, the width is 5 km (as for model 1) and the NE limit is marked by the Cougne Fault, which in this case is considered as being involved in the thermal flow. The maximum thickness of the three blocks modeled is fixed at 5.5 km, assuming that this value represents the approximate depth at which thermal water equilibration occurs (*c*. 150 °C, if a gradient of 30 °C km^{-1} is

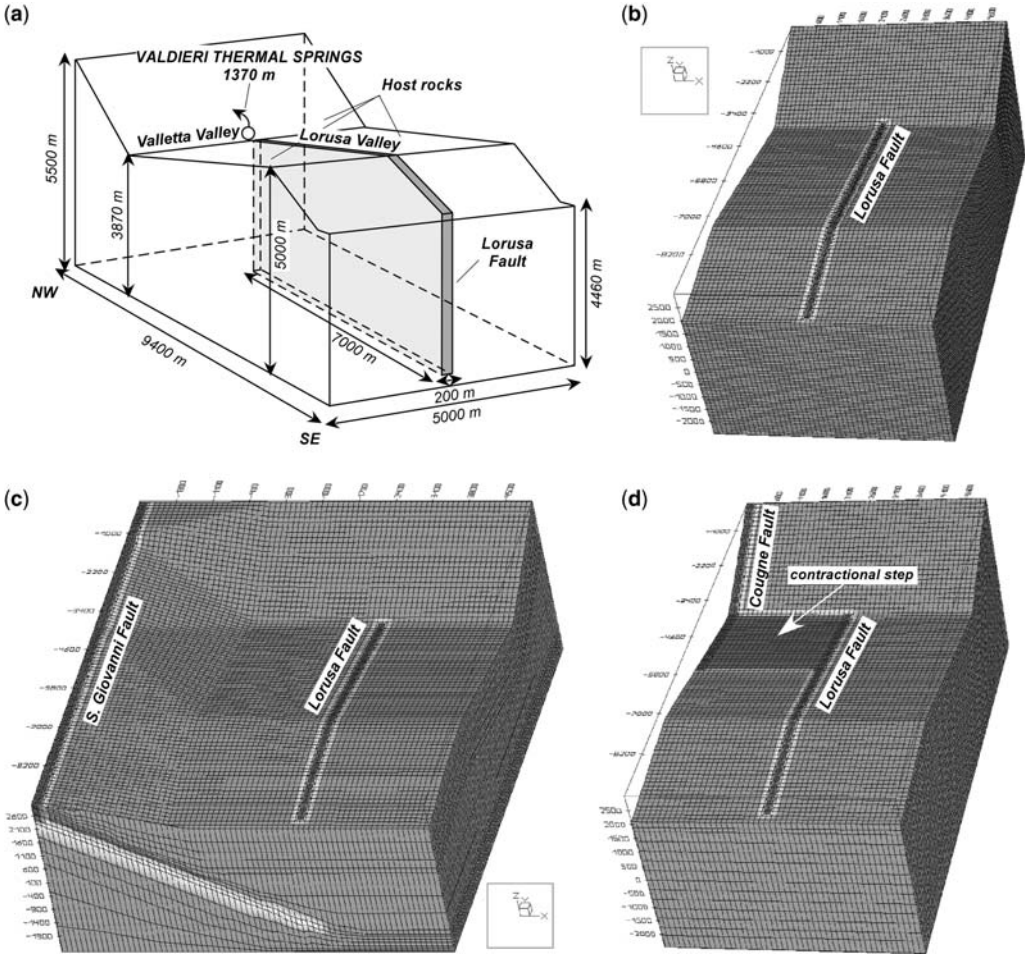

Fig. 3. 3D geometry and dimensions used for the numerical simulations. (**a**) Dimensions of the base geometry of model 1. A vertical fault plane, 200 m wide and 7 km long, representing the damage zone of the Lorusa Fault, is enclosed within a block of host rocks. The maximum thickness of the modeled block is fixed at 5.5 km, assuming that this value represents approximately the depth at which thermal water equilibration occurs. Discretized elements of model 1 (**b**), model 2 (**c**) and model 3 (**d**) are shown.

assumed; Perello *et al.* 2001). In all the geometries, the elements are composed of cubic cells with a horizontal size of 100 × 100 m within the protolith rocks. To provide sufficient resolution of both thermal and flow regimes along the faults, the cell size is halved (50 × 50 m) in those areas. The computer software used to perform the simulations is the three-dimensional Galerkin finite-element program, FeFlow® 5.1 (Diersch 1998).

The simulation results were calibrated by comparing the numerical outputs with spring temperatures of 70 °C and flow rates of 50 kg s^{-1} (*c.* 4320 m^3/day). As an additional condition, it was sought to achieve a close fit between the simulated temperatures and the 20 °C reading that was taken within the Ciriegia tunnel connected to the Lorusa Fault. It must be emphasized that after the drilling of the tunnel in 1960, no significant perturbation was recorded in subsequent years at the springs. Tests on the sensitivity of the thermal flow system to the presence of the tunnel were carried out for all three model geometries by introducing in an appropriate location a fluid sink of 15 kg s^{-1} for a time span of 100 years. In all models tested, the presence of the tunnel itself did not cause any significant perturbation to the thermal circulation (*c.* 1 °C variation at the springs), so this factor was not considered further in the simulations.

In general, modelling was performed in two stages: (1) thermo-hydraulic simulations were first carried out in a steady-state regime; (2) these results were then taken as initial conditions for a coupled fluid flow and heat transport simulation in a transient regime. This procedure implicitly assumes that a circulation system was already active and that it accounted for a steady-state pressure–temperature distribution. Despite considerable uncertainty regarding this assumption, adopting initial steady-state conditions is a convenient approach that allows comparison of the temporal responses of the thermal circulation in the different systems modelled (cf. also McKenna & Blackwell 2004). Three-dimensional computations, especially those performed in transient regimes, are time-consuming. A simulation timespan of 10 000 years was chosen as it allowed a relatively high number (*c.* 100) of tests on transient-regime models to be performed.

The thermo-hydraulic behaviour of fault-related geothermal systems is commonly affected by processes that can involve either an increase or a decrease in fault permeability (Parry 1998) or the creation of fluid density and viscosity dependencies on temperature and salinity (Simms & Garven 2004). These processes result in changes to the groundwater flow patterns over time. Therefore, transient-regime as opposed to steady-state simulations provide, in principle, better approximations of thermal flow systems. To understand fully how temporal variations in permeability occur within a thermal system, a good characterization of the processes underlying these variations should first be attempted.

Microstructural observations suggest that the Lorusa Fault has been affected by repeated episodes of cataclasis, fluid influx and cementation, reflecting cycles of permeability increase and decrease (Baietto 2007). However, the kinetics of crack sealing with respect to the rate of geodynamic processes occurring in the Valdieri sector are unknown. The assessment of these parameters would require modelling of the sensitivity of crack sealing to various parameters, as performed by Gratier *et al.* (2003), but this exercise is beyond the scope of the present study. Instead, permeability was assumed to be constant over time, and transient-regime simulations were performed by solving coupled fluid and heat flow equations, which in turn permitted verification of the natural conditions giving rise to thermal convection. The mass conservation equation for the fluid phase is

$$\frac{\partial(\phi\rho)}{\partial t} + \nabla \cdot \rho\mathbf{q} = 0 \tag{1}$$

where ϕ is the porosity of the medium (dimensionless), ρ is the fluid density (kg m^{-3}), ∇ is the divergence operator and $\mathbf{q}$ is the flux vector (m s^{-1}). The latter quantity obeys Darcy's law,

$$\mathbf{q} = -\frac{\mathbf{k}}{\mu}(\nabla p + \rho\mathbf{g}) \tag{2}$$

where $\mathbf{k}$ is the permeability tensor of the medium (m^2), $\mathbf{g}$ is the acceleration due to gravity (m s^{-2}), μ the dynamic fluid viscosity (kg $m^{-1}s^{-1}$), and p the pore pressure (N m^{-2}). In the context of coupled flow and heat transport processes, both fluid density and viscosity vary with temperature T according to the appropriate constitutive laws $\rho = \rho(T)$ and $\mu = \mu(T)$ as given in equation (4). The conservation equation for advective–dispersive–diffusive transport of thermal energy is

$$[\phi(\rho c)\mathrm{l} + (1-\phi)(\rho c)\mathrm{s}]\frac{\partial T}{\partial t} + (\rho c)\mathrm{l}\mathbf{q} \cdot \nabla T = \nabla \cdot [\phi\Lambda\mathrm{l} + (1-\phi)\lambda\mathrm{s}\mathrm{I}]\nabla T \tag{3}$$

where (ρc)l and (ρc)s are the volumetric heat capacities (J m^{-3} K^{-1}) of the liquid and solid phases, respectively. In equation (3), $\lambda s\mathbf{I}$ (J $m^{-1}s^{-1}$ K^{-1}) is the thermal conduction tensor of the solid phase (assumed isotropic), and

Λl ($\mathrm{J\,m^{-1}s^{-1}\,K^{-1}}$) the hydrodynamic thermal dispersion tensor of the fluid phase. Equations (1) and (2) can be further developed to yield a governing flow equation in terms of pore pressure. Introducing the arbitrary temperature T_0, at which $\rho_0 = \rho$ ($\mathrm{T_0}$) and $\mu_0 = \mu$ (T_0), Darcy's law in equation (2) can be re-written as

$$\mathbf{q} = -\frac{\mathbf{k}\rho_0 g}{\mu_0}\frac{\mu_0}{\mu}\left(\nabla\frac{p}{\rho_0 g} + \frac{\rho}{\rho_0}\nabla z\right) = -\mathbf{K}_0\frac{\mu_0}{\mu}\left(\nabla H_0 + \frac{(\rho-\rho_0)}{\rho_0}\nabla z\right) \qquad (4)$$

where $\mathbf{K}_0 = \mathbf{k}\rho_0 g/\mu_0$ ($\mathrm{m\,s^{-1}}$) is the hydraulic conductivity tensor at $T = T_0$ and $H_0 = \mathrm{p}/\rho_0 g + z(\mathrm{m})$ is a notional hydraulic head, also at T_0. To allow the use of more conventional hydrogeological parameters such as hydraulic conductivity and specific storage, the equivalent hydraulic head formulation in equation (4) is used in this paper. The only coupling laws considered are temperature-dependent functions for both fluid viscosity and density. Fluid salinity is not considered owing to the low salinity of the Valdieri waters ($<0.4\ \mathrm{g\,l^{-1}}$; Perello *et al.* 2001). To compute the fluid viscosity, a polynomial expression for the hydraulic conductivity correction factor, μ_0/μ, derived from Mercer & Pinder (1974) is introduced in equation (4). To express the variation of fluid density with temperature, a conventional form is: $\rho(T) = \rho_0[1 - \beta(T)(T-T_0)]$, where $\beta(K^{-1})$ is the volumetric thermal fluid expansion coefficient and ρ_0 the reference fluid density. In a geothermal context where large temperature variations can be expected and buoyancy forces dominate, β varies widely. In the present simulation, a calculation of a non-linear temperature-dependent expansion coefficient β is included, based on the physically 'exact' fluid density curve measured in the range 0–100 °C (Perrochet & Tacher 1997). The temperature and pressure fields obtained from steady-state simulations are used with the boundary conditions to solve equations (3) and (4) simultaneously. In the calculations, the so-called 'Boussinesq approximation' is adopted as usual for most density-dependent transport phenomena (Bird *et al.* 1960). This allows a simplification of the coupled nonlinear systems of mass and energy balance equations, but without the elimination of intrinsic coupling mechanisms which are significant for thermal convection. Automatic time-step control was carried out by the Adams–Brashfort/Trapezoidal-rule predictor–corrector scheme. Sequential Picard iteration between flow and heat transport is used to accommodate the nonlinearities resulting from variable-density flow.

A description of flow through fractured systems would require exact information about each individual fracture, which in practice is almost never available. Hence, in practice such environments can be only described in terms of *equivalent porous media*. This type of assumption was adopted here and is widely employed when simulating faulted systems (e.g., Garven *et al.* 2001; Simms & Garven 2004; Wisian & Blackwell 2004; McKenna & Blackwell 2004). Simulation parameters used in this work are shown in Table 1; note that the term 'fault' is used for all faults that are taken into account in each of the model geometries considered, including the jog in model 3. Many of these parameters and boundary conditions were based by necessity on generalized assumptions and simplifications. Sensitivity studies were used mainly to determine the effect on the hot-spring response of varying the fault and host rock permeability, but sensitivity tests were also carried out on some other parameters, such as basal heat flux, host rock porosity and infiltration rates, as described later in this paper.

Table 1. *Typical simulation parameters used in the three geometries modelled*

Parameter	Value
Fault permeability	1×10^{-12} to 1×10^{-15} $\mathrm{m^2}$
Host rock permeability	1×10^{-13} to 1×10^{-18} $\mathrm{m^2}$
Fault porosity	0.1
Host rock porosity	0.01–0.1
Solid thermal conductivity	3.0 $\mathrm{J\,m^{-1}\,K^{-1}\,s^{-1}}$
Solid thermal capacity	2.28×10^{6} $\mathrm{J\,m^{-3}\,K^{-1}}$
Fault infiltration rate	1.7×10^{-4} m/day
Host rock infiltration rate	1.7×10^{-5} m/day
Basal heat flow	80–100 $\mathrm{mW\,m^{-2}}$
Altitudinal temperature gradient	0.004 °C $\mathrm{m^{-1}}$
Heat production	2.5μW $\mathrm{m^{-3}}$
Longitudinal thermal dispersivity	10
Transverse thermal dispersivity	100

Permeabilities in the range of 10^{-18}–10^{-12} m^2 were used in these simulations because these values can be considered as representative of most rocks of the upper continental crust (Manning & Ingebritsen 1999). To reproduce the tendency of the Valdieri faults to act as partial barriers to fluid crossflow (Baietto 2007), these faults were assigned one order of difference in magnitude between the permeability oriented parallel to the fault and the permeability oriented normal to the fault surface. The permeability of both faults and host rocks is assumed to be isotropic along the vertical direction. More likely situations in which bulk rock permeability decreases with depth (e.g., exponentially, cf. Ingebritsen and Manning 1999) will be investigated in subsequent modelling. A constant and isotropic thermal conductivity of 3.0 W m^{-1} K^{-1} was applied to the bulk of the modelled block, because this is representative for granitic rocks (Chapman & Furlong 1992). The heat capacity of the modelled rock mass was set to 2.28×10^6 J m^{-3} K^{-1} and the heat production to 2.5 μW m^{-3}, which are typical values for a granitic crust (Rybach 1981). Porosity was set at 0.1 through the fault zone, while in the host rocks it was varied from 0.01 to 0.1, which is a representative range for moderately to intensely fractured crystalline rocks (Brace *et al.* 1966). The conductivity, diffusivity, density and heat capacity (solid and fluid) are kept constant over time and are assumed to be independent of temperature.

Concerning the hydraulic boundary conditions, the lateral boundaries of the three models were set as impermeable to fluid and heat flow. In all models, a free-surface computation has been applied to the upper topographic boundary. This approach provides an appropriate condition to reproduce reasonable recharge patterns through the system (Forster & Smith 1989). The FeFlow software provides an advanced method which is based on 3D moving meshes, allowing for more accurate and rigorous modelling of heat processing compared with a computation based on fixed grids (Diersch 1998). Even if the recharge rates in the Terme di Valdieri zone are unknown, this approach enables constraint of the water table by incorporating the imposed infiltration rates into the computations. In all models, a hydraulic head corresponding to an altitude of 1370 m was imposed at the lowermost part of the topographic surface to reproduce the river running through the Valletta valley. On the rest of the upper boundary, infiltration rates of 1.7×10^{-4} and of 1.7×10^{-5} m/day were assigned at the surface of faults and of host rocks respectively. These values were selected after estimation procedures based on average rainfall in the Valdieri area (about 1400 mm a^{-1}; Regione Piemonte database) and on preliminary sensitivity tests aimed at evaluating the consistency of the fluid pressure field with respect to the Ciriegia tunnel. Furthermore, these conditions are also consistent with the infiltration rates that Forster & Smith (1989) used in their models to simulate the groundwater flow in a mountainous setting similar to that of Terme di Valdieri. However, since these infiltration values are based only on indirect evaluations, the sensitivity of these values to changes of up to an order of magnitude was analysed and is discussed below.

A Cauchy-type temperature condition controlled by heat transfer coefficients is imposed along the fault trace and at the valley bottom (1370 m). This condition allows for the continuity of the heat flux across the boundary and control of surface temperatures by rising groundwater. On the upper surface of the host rocks, temperatures are fixed according to an altitudinal gradient of 0.004 °C m^{-1}. The Valdieri station has a reference mean temperature of 7 °C. Basal heat flows (BHF) of 80 and 100 mW m^{-2} were imposed at the lowest altitude of the models. These values seem appropriate for the region of Valdieri, where high exhumation rates (*c.* 1.3 mm a^{-1}) have been recorded for the past 3.5 Ma (Bigot-Cormier *et al.* 2000). Jaboyedoff & Pastorelli (2003) estimated that regions undergoing exhumation at rates of 1 mm a^{-1} can have heat flow densities on the order of the values here attributed to Valdieri.

Model 1: single-conduit v. fracture network model

In this model, the Lorusa Fault is assumed to constitute the main channel for fluid flow. Accordingly, a focused flow occurs if most of the fluid flows through this fault and a negligible contribution comes from the surroundings (i.e., the single-conduit model). Conversely, fluid flows pervasively if the permeability of the fractured host rocks is sufficiently high to allow advection from the surroundings. In this case, the circulation in the Lorusa Fault can result from the combination of fluids infiltrating directly from the fault surface and fluids migrating in from the fault zone wallrocks (i.e., the fracture network model). As can be deduced from Figure 3a, the amount of fluid flow directed towards the Lorusa Fault from the host rock depends both on the capability of the fault to draw fluids and of the host rocks to allow fluids to circulate. In other words, focused as opposed to pervasive flows are expected to occur as the result of different host rock and fault equivalent permeabilities. Sets of steady-state and transient-regime simulations are performed here

to investigate dependencies among specific heat and fluid flow regimes on different fault and host rock permeabilities.

Steady-state simulation

Figure 4a & b shows contours in permeability space of the percentages of fluid and heat fluxes discharging at springs, compared respectively with the total fluid fluxes penetrating across the topographic surface and with the heat fluxes imposed at the base of the model. These diagrams provide a first approximation to constraints on the sensitivity of spring temperatures and discharges to fault permeability (k_f) and host rock permeability (k_{hr}). Since the contours express relative percentages, Fig. 4a & b holds true for BHF values of both 80 and 100 mW m^{-2}. Figure 4a shows evidence of the dependency of the proportion of total fluid discharged at the spring on the host rock permeability. For $k_{hr} = 1 \times 10^{-16}$ m^2, the fluid discharge exceeds 90% of total mass, whereas for permeabilities lower than 1×10^{-16} m^2, the amount of fluid discharged decreases to values of 30–40% of total mass. This variation is related both to the limited fluid recharge capacity of the host rock – because infiltration is constrained by hydraulic head – and to the fact that as the water table rises, increasing amounts of fluid flow out of the system instead of reaching the springs. For values of k_{hr} higher than 1×10^{-16} m^2, owing to the reduced permeability difference between the host rock and the fault, the draining effect of the fault decreases, with a consequent decrease in the amount of fluid upwelling at the springs. Conversely, discharge rates are less affected by k_f. This can be explained by the fact that the infiltrations imposed at the fault surface percolate within the fault, with relatively little dispersion into the surroundings. At values of k_f lower than 5×10^{-14} m^2, the fluid discharge is reduced because of the decreased drainage capacity of the fault. In terms of absolute fluid rate, a discharge peak of 1205 m^3/day is reached at $k_{hr} = 1 \times 10^{-16}$ m^2 and $k_f = 1 \times 10^{-12}$ m^2, with 80% of the fluid supply derived from the host rock. However, this is about 3.6 times less than the expected rate for the Valdieri springs, and thus this condition does not provide the required quality of fit.

The contours shown in Figure 4b indicate that the percentage of heat discharged at the springs depends both on the host rock and on the fault zone permeability. The maximum percentage of heat reaching the springs exceeds 50% of the total available heat in the permeability range 3×10^{-17} to 3×10^{-16} m^2, for the host rock, and 2×10^{-13} to 8×10^{-13} m^2, for the fault itself. Compared with the contour distribution of the fluid discharges, a more restricted k_f range is required in order to achieve a heat flux peak of waters released at the spring. In fact, at lower fault and host rock permeabilities, fluid flow to the fault is limited, and a greater proportion of basal heat flow is transferred by conduction to the surrounding rock, while at higher fault and host rock permeabilities, the amount of discharged heat is less because a larger volumetric flux stores most of the thermal energy imposed at the base of the system. Within the

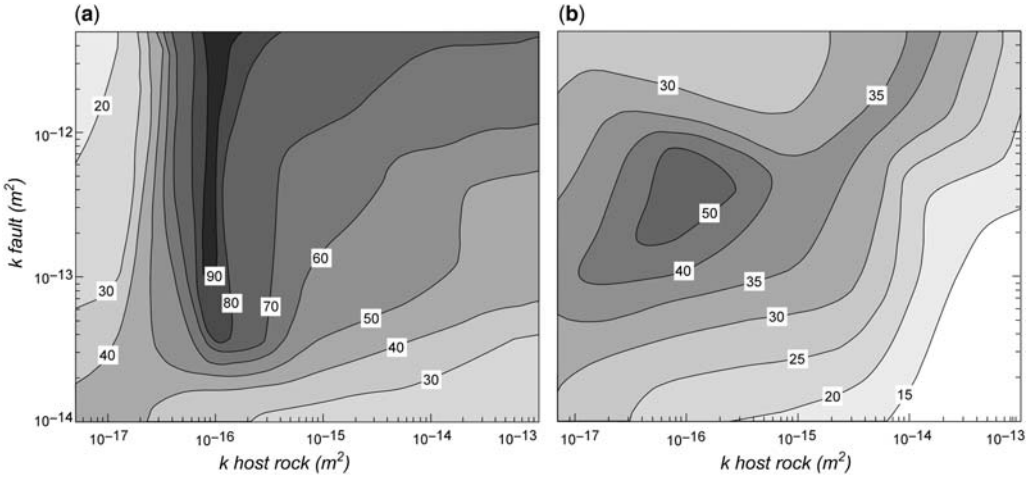

Fig. 4. Results of steady-state simulations using model 1. (**a**) Contours indicating the percentage of fluid flux discharging at the springs relative to the infiltration rates imposed on the upper (topographic) boundary of the system. (**b**) Contours indicating the percentage of heat flux discharging at the springs relative to the bulk heat flux imposed on the system. Plots are expressed on a logarithmic scale as a function of the fault and host rock permeabilities.

50% contour, at a BHF of 80 mW m^{-2}, the peak water temperature is 52 °C, while at 100 mW m^{-2}, the peak temperature increases to 62 °C.

Figure 5a illustrates the distribution of isotherms across the fault profile obtained with a BHF of 80 mW m^{-2}, $k_f = 2 \times 10^{-13}$ m^2 and $k_{hr} = 1 \times 10^{-16}$ m^2. At the fault base, the steady-state solution indicates that temperatures are approximately 130 °C, with a maximum ΔT of 15 °C with respect to the surrounding rocks. Under the same conditions, and with a heat flux of 100 mW m^{-2}, the temperature at the fault base increases to 160 °C (Fig. 5b). The latter result gives a thermal distribution through the fault which is reasonably consistent with the temperature of 150 °C that was estimated for the base of the reservoir, and with the 20 °C encountered within the Ciriegia tunnel. However, the steady-state solutions predict spring discharges that are not consistent with the measured spring rates. Since the imposed calibration procedure requires a simultaneous fit of both discharge rates and temperatures with those measured at the springs (i.e., $T = 70$ °C; $Q = 4320$ m^3/day), the hydraulic and thermal numerical results cannot be improved independently simply by increasing or decreasing the rate of fluid penetration through the system. For instance, if the infiltration rates are increased by one order of magnitude (i.e., 1×10^{-4} and 1×10^{-3} m/day, respectively, on top of the host rocks and in the fault), the expected value of 4320 m^3/day can be attained at the springs (for $k_f = 2 \times 10^{-13}$ m^2 and $k_{hr} = 1 \times 10^{-16}$ m^2). However, in this case the outlet spring temperatures would be too low, reaching only 40 and 51 °C respectively for BHF of 80 and 100 mW m^{-2}. In addition, in both cases, the isotherms would remain excessively depressed by comparison with the temperatures found in the Ciriegia tunnel and the temperatures expected at the base of the system.

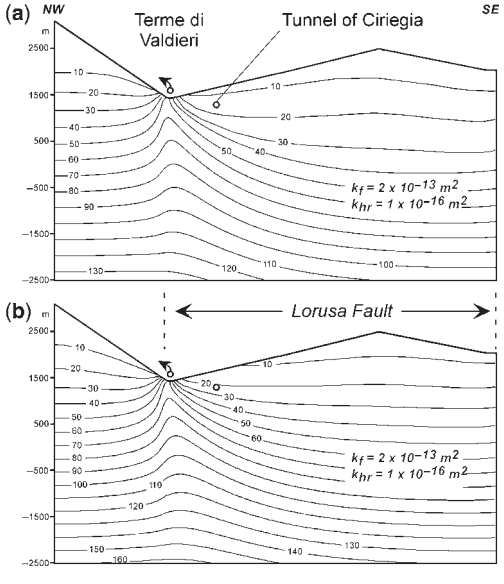

Fig. 5. Steady-state distribution of isotherms across the fault profile obtained for permeabilities of 2×10^{-13} and 1×10^{-16} m^2 of the fault (k_f) and host rock (k_{hr}), respectively. Isotherm distribution obtained with a basal heat flow of 80 (**a**) and 100 mW m^{-2} (**b**).

Transient-regime simulation

The transient-regime simulations show that, at sufficiently high fault permeabilities, convective circulation can occur in the Lorusa Fault. Similarly to the results shown in Figure 4b, the transient results are examined using as a reference the contours in permeability space of the heat flux percentages discharging at the spring site with respect to the total heat fluxes imposed on the models. Figure 6a–6d shows the contours for simulation times of 10, 100, 1000 and 10 000 years, respectively, at a BHF of 80 mW m^{-2} (solutions with a BHF of 100 m W m^{-2} are discussed later). After 10 years (Fig. 6a) from circulation onset, the heat flux distribution in the permeability space changes noticeably compared with the steady-state distribution, with a proportion of heat delivered at springs as high as 20% of the applied heat. The region where this peak occurs is between fault permeabilities of 7×10^{-14} and 3×10^{-14} m^2 and host rock permeabilities of 2×10^{-16} and 1×10^{-16} m^2, indicating that the peak region has both been restrained and has shifted toward lower permeabilities in the fault zone. The shift in position and magnitude of the heat flux peak within the permeability field reflects the perturbation recorded by the steady-state flow system owing to the introduction of temperature dependencies on density and viscosity. After 100 years (Fig. 6b), the heat flux peak records a further decrease in magnitude (max. 14%) and a further shift in spatial permeability distribution. However, it should be noted that, for k_f higher than 5×10^{-13} m^2, increasing amounts of groundwater are discharged at the springs. A peak of discharged heat (33%) occurs at $k_f = 1 \times 10^{-12}$ m^2 and $k_{hr} = 2 \times 10^{-17}$ m^2. For k_{hr} higher then 3×10^{-16} m^2, the heat discharge decreases because of a greater proportion of cold shallow waters flowing in from the host rock towards the fault and then upwelling at the springs. After 1000 years (Fig. 6c), the peak region broadens and the contour distribution indicates a dependency of heat discharge maxima on fault permeability. Amounts exceeding 80% of the imposed heat flux are obtained for a

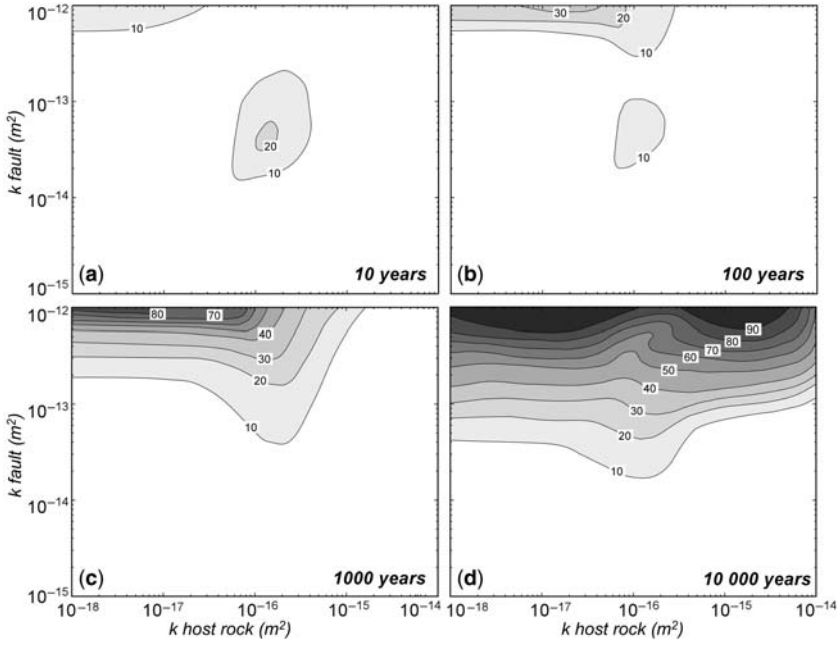

Fig. 6. Transient-regime results for model 1, plotted in permeability space. The contours represent the heat flux percentages discharging at the spring site with respect to the total heat fluxes imposed on the models after (**a**) 10, (**b**) 100, (**c**) 1000 and (**d**) 10 000 years since circulation onset.

$k_f = 1 \times 10^{-12}$ m^2, while the positive peak can be rapidly decreased by 10% if the permeability is decreased by an order of magnitude. Increased effects of discharged heat occur for k_{hr} in the range of 4×10^{-16} and 5×10^{-17} m^2, due to the enhanced capability of the host rocks to convey, at these permeabilities, a large amount of heated fluids along the fault plane. After 10 000 years (Fig. 6d), the region containing peaks of heat discharges further broadens towards lower fault permeabilities, and the proportion of discharged heat increases compared with previous stages.

These results were also analysed to estimate the influence of the fault and host rock permeability on the types of fluid flow and heat transfer regimes that occur within the geothermal system. Figure 7 shows the regions in the permeability field where advection, conduction and convection are the dominant processes within the fault and host rocks at BHF values of 80 and 100 mW m^{-2}. The transition between an advective regime and a convective regime was identified by completing a series of simulations at constant host rock permeability and variable fault permeabilities. For BHF values of 80 and 100 mW m^{-2}, conduction is the predominant heat transfer process within the host rocks

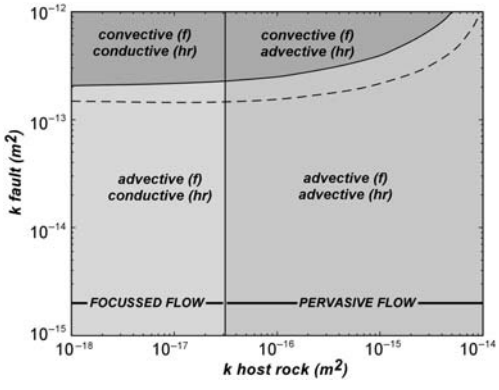

Fig. 7. Thermal regimes of the fault (f) and of the host rocks (hr) plotted in permeability space for model 1. At permeability less than 3×10^{-17} m^2, the host rocks transfer the heat by conduction and the thermal circulation is mainly focused within the damage zone of the Lorusa Fault. Above this value, the thermal circulation results from a combination of focused flow within the fault and pervasive flow through fractures within the host rocks. The region where thermal convection occurs within the fault zone is represented in dark grey (BHF = 80 mW m^{-2}). The dotted line represents the boundary of this field for a BHF = 100 mW m^{-2}.

only at permeabilities lower than 3×10^{-17} m^2, while at higher values, advection becomes the dominant process. This makes it possible to distinguish between two fields where the fractures within the host rock are, or are not, hydraulically connected. At permeability values below 3×10^{-17}m^2, heat is transferred predominantly by conduction as most fractures are not connected, while above this value, advection prevails, reflecting the fact that the fractures have attained a percolation threshold so that pervasive flow occurs. In this regime, the proportion of fluids flowing from the host rocks to the fault plane and finally discharged at the springs becomes a function of the fault drainage capability. For example, this capability was estimated by comparing the total cumulative amount of spring discharges during 10 000 years of thermal activity for a fixed k_{hr} of 1×10^{-16} m^2 and a variable k_f in the range from 5×10^{-15} to 5×10^{-13} m^2. At $k_f = 5 \times 10^{-15}$ m^2 the drainage is negligible; at $k_f = 5 \times 10^{-14}$ m^2 the fault draws 27% of the fluid mass circulating in the surrounding country rock; this percentage increases to 57 and 71% if the k_f is increased to 1×10^{-13} and 5×10^{-13} m^2, respectively. Accordingly, the maximum distance of drainage from the fault increases from 1100 m ($k_f = 5 \times 10^{-14}$ m^2) to 1500 m ($k_f = 1 \times 10^{-13}$ m^2) and to 2100 m (5×10^{-13} m^2).

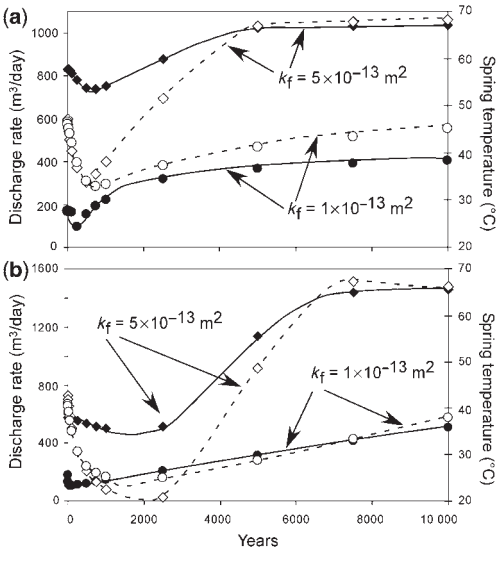

Fig. 8. Maximum flow rates and temperatures of waters discharging at springs v. time in years, plotted for $k_f = 1 \times 10^{-13}$ and 5×10^{-13} m^2 and host rock permeabilities of (**a**) 1×10^{-17} and (**b**) 1×10^{-15} m^2 using model 1. The BHF is 80 mW m^{-2}. Symbols (•) and (◆) represent water discharges, while (○) and (◇) represent maximum spring temperatures.

Within the fault, the transition between advection and convection was identified by completing a series of simulations at constant host rock permeability and variable fault permeabilities. Figure 7 shows that as the host rock permeability is increased, the convective cells onset within the fault at slightly higher fault permeabilities. At $k_{hr} = 1 \times 10^{-18}$ m^2, this onset occurs at $k_f = 2 \times 10^{-13}$ m^2, while at $k_{hr} = 5 \times 10^{-18}$ m^2, it occurs at $k_f = 1 \times 10^{-12}$ m^2. The effect of increasing the BHF from 80 to 100 mW m^{-2} is to expand the convective field toward lower values of fault permeability and higher values of host rock permeability. Figure 8a and b provides an illustration of the spring flow rate and temperature variation over time for two cases: (a) $k_f = 1 \times 10^{-13}$, $k_f = 5 \times 10^{-13}$ m^2, and $k_{hr} = 1 \times 10^{-17}$, and (b) $k_{hr} = 1 \times 10^{-15}$ m^2 with the other values unchanged, illustrating the difference in spring response to advective and convective flow systems. It can be noticed that: (i) a negative trend in flow rates and temperatures occurs during the initial stages of circulation, and the negative trend in temperature is more pronounced at higher fault permeability; (ii) at higher fault and host rock permeabilities (Fig. 8b), the negative temperature anomaly persists for a longer period than at lower permeabilities; (iii) after 10 000 years, the thermal and hydraulic spring outputs are mainly contingent on fault permeabilities, such that an enhancement in k_f from 1×10^{-13} to 5×10^{-13} m^2 brings about a marked increase in the discharge temperatures and flow rates for both the modelled host rock permeabilities; and (iv) quasi-steady-state configurations are attained at lower host rock permeabilities. During initial periods of simulated circulation [points (i) and (ii)], the flow rates and temperatures decrease because of the bulk rearrangement of the circulation patterns related to the introduction of density and viscosity dependencies on temperature. This negative anomaly lasts for a longer time at higher host rock permeabilities, because the springs discharge proportionally higher amounts of cold water which infiltrates in from the nearby host rocks. The considerable increment in discharge temperature and discharge flow rate [point (iii)] recorded by increasing the fault permeability from 1×10^{-13} to 5×10^{-13} m^2 reflects the efficiency of the convective circulations (active within the fault at 5×10^{-13} m^2) in bringing a larger amount of fluid and heat toward the surface. By contrast, the onset of a convective circulation is not achieved with an imposed k_f of 1×10^{-13} m^2, resulting in lower proportions of heat and flow reaching the surface. More stable configurations [point (iv)] arise at lower host rock permeability because the self-rearrangement of the circulation patterns

occurs mainly within the fault plane. Figure 9 shows the isotherm distribution along the Lorusa Fault at 2500 years and 10 000 years for $k_f = 5 \times 10^{-13}$ m^2 and $k_{hr} = 1 \times 10^{-15}$ m^2 respectively. Moreover, the efficiency of the convective circulations in conveying heat toward the surface can be estimated by inspection of Figure 10, which shows the isosurface corresponding to a temperature of 70 °C at 10 000 years for different fault permeabilities and for a fixed host rock permeability of 1×10^{-17} m^2. As k_f varies from 1×10^{-14} to 1×10^{-13} m^2, the hot plume located below the spring site is slightly amplified. As k_f varies from 1×10^{-13} to 5×10^{-13} m^2, the isosurface changes dramatically in shape owing to the development of convection that gives rise to a positive thermal anomaly that intercepts the topographic surface at the spring site.

Despite the detailed characterization of the hydraulic and thermal state of the Valdieri system model, none of the combinations of fault and host rock permeabilities in the regimes shown in Figure 7 satisfies the required conditions for calibration. In fact, the simulated spring discharges are underestimated with respect to the expected values of flow rates measured at Valdieri, even considering the highest-performing case: at $k_{hr} = 1 \times 10^{-15}$ m^2 and $k_f = 1 \times 10^{-12}$ m^2, after 7500 years from circulation onset, the spring temperature ($T_{sim} = 69$ °C) fulfills the calibration condition ($T = 70$ °C), while the discharge rate ($Q_{sim} = 2248$ m^3/day) represents only about half the expected value ($Q = 4320$ m^3/day). In the convective flow region, moderate, but still insufficient improvements in the results are obtained for models based on a BHF of 100 mW m^{-2}. In summary, this discussion has revealed that the numerical models representing combinations of a single-conduit geometry surrounded by hydraulically connected fracture networks do not give a reasonable description of the Terme di Valdieri circulation system.

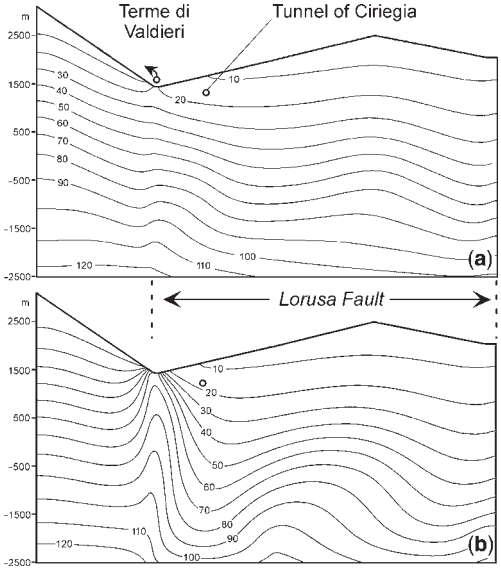

Fig. 9. Isotherm distribution across the Lorusa Fault obtained for $k_f = 2 \times 10^{-13}$ m^2 and $k_{hr} = 1 \times 10^{-15}$ m^2 using model 1. (**a**) Distribution after 2500 years and (**b**) after 10 000 years.

Model 2: fault intersection

This scenario includes the interception at depth of the Lorusa Fault by the S. Giovanni Fault (Fig. 2), and both structures contribute to the thermal flow feeding the Terme di Valdieri springs. The two faults show a comparatively similar proportion of damage/core zone, which suggests that they share broadly equivalent hydraulic properties. Ideally, pressure gradients due to the higher topographic elevation of the S. Giovanni Fault with respect to the Lorusa Fault would drive fluids through the two faults and then up to the surface at the thermal springs. The model geometry represented in Figure 3c was used for performing sensitivity tests of the Lorusa and S. Giovanni fault permeabilities on spring temperatures and flow rates. Since this model aims mainly to identify the impact of fault linkage on the bulk thermal system, simulations were carried out with a fixed host rock permeability of 1×10^{-15} m^2 and with an equal permeability value and a constant infiltration rate of 1.7×10^{-4} m day^{-1} assigned to both

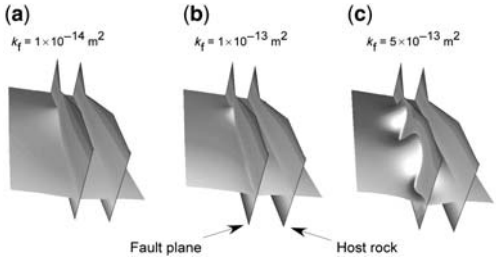

Fig. 10. Isosurface corresponding to a temperature of 70 °C (at $t = 10\,000$ years) obtained using model 1 for a fixed host rock permeability of 1×10^{-17} m^2 and fault permeabilities of (**a**) 1×10^{-14} m^2, (**b**) 1×10^{-13} m^2 and (**c**) 5×10^{-13} m^2. Heat fringes traced along the fault plane and within the host rock are also displayed. It can be noticed that the onset of convective circulation cells occurs between 1×10^{-13} and 5×10^{-13} m^2 and that the effects of convection strongly perturb the thermal state of the surrounding protolith rocks.

faults in each simulation run. Figure 11 shows the evolution over time of spring flow rate and temperature, with $k_f = 1 \times 10^{-13}$, $k_f = 5 \times 10^{-13}$ m^2, and $k_{hr} = 1 \times 10^{-15}$. Compared with the trends shown in Figure 8, this diagram shows that the two faults intercepting at depth increase the bulk discharge, but decrease the maximum temperature. After 10 000 years, at $k_f = 1 \times 10^{-13}$ m^2, the discharge rate is approximately 800 m^3/day at a temperature of 46 °C. If a $k_f = 5 \times 10^{-13}$ m^2 is imposed, the discharge rate doubles owing to the increased drainage from the S. Giovanni Fault of the fluids flowing adjacent of this zone, but the temperature rises only to 42 °C. This behaviour occurs because fluids infiltrating through the S. Giovanni Fault contribute to a relatively rapid increase (in a few tens of years) of the total fluid flow within the Lorusa Fault, but remove more heat at the base of the thermal system when compared with the case where the two faults were not linked (cf. Fig. 8b). The advective perturbation caused by the fluid flow within the S. Giovanni Fault inhibits the onset of convective circulations in the Lorusa Fault, which results in lower discharge temperatures. Figure 12a & b illustrate the isotherm distribution within the Lorusa Fault at $k_f = 5 \times 10^{-13}$ m^2 at 2500 and 10 000 years respectively. At both simulation times, the presence of the S. Giovanni Fault causes a separation of the isotherm distribution above the zone of linkage, with apparent geothermal gradients of *c*. 15 °C km^{-1}, and below the zone, with apparent geothermal gradients exceeding 40 °C km^{-1}. It must be remarked that no significant improvement of the numerical results with respect to the calibration conditions was achieved by varying fault or host rock permeabilities. Moreover, assuming a BHF = 100 mW m^{-2}, it does not lead to a definitive solution of the problem, because it results in spring temperatures which are slightly increased (maximum 57 °C over 10 000 years), but still distant from the required values. Even simulations carried out with lower permeabilities for the S. Giovanni Fault with respect to the Lorusa Fault produced no significant improvement. In summary, these results indicate that a fault linkage scenario has difficulty explaining the measured values at the Terme di Valdieri springs.

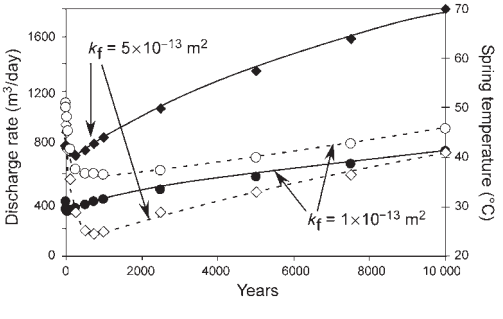

Fig. 11. Maximum flow rates and temperatures of waters discharging at springs v. years, plotted for fault permeabilities of 1×10^{-13} and 5×10^{-13} m^2 and host rock permeabilities of 1×10^{-15} m^2 using model 2. The BHF is 80 mW m^{-2}. Symbols (•) and (◆) represent water discharges, while (○) and (◇) represent maximum spring temperatures.

Model 3: fault interaction

The springs of Terme di Valdieri are sited in an area of fracturing that corresponds to a contractional step-over developed by the interaction of the Lorusa Fault with the Cougne Fault. As with model 2, the thermal flow can be partitioned between two faults that act as separate channels. However, in this case, waters circulating in the two systems can come into contact through the jog rather than by direct fault linkage. This implies that the resulting thermal flow system would depend not only on the hydraulic properties of the Lorusa and Cougne Faults, but also on the specific hydraulic properties, such as the fracture hydraulic connectivity, of the breakdown region between these two faults. The model geometry represented in Figure 3d was used as a basis for

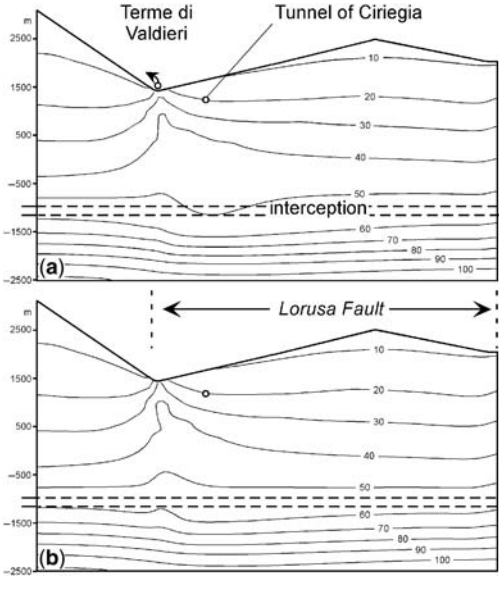

Fig. 12. Isotherm distribution across the Lorusa Fault obtained for $k_f = 5 \times 10^{-13}$ m^2 and $k_{hr} = 1 \times 10^{-15}$ m^2 using model 2. (**a**) Distribution after 2500 years and (**b**) after 10 000 years.

performing sensitivity tests for the Lorusa Fault, the Cougne Fault, and the effect of jog permeabilities on spring temperatures and flow rates. Figure 13 shows the differences in response of spring temperatures and discharges due to advective as opposed to convective flows. As in the previous models, fault permeability was set equal to 1×10^{-13} and 5×10^{-13} m^2, while the host rock permeability was kept fixed at 1×10^{-15} m^2. Accordingly, the permeability of the region corresponding to the step-over was set equal to that attributed to the faults. After 500 years, at $k_f = 1 \times 10^{-13}$ m^2, the springs record a linear increase of temperatures and discharges that attain, at 10 000 years, values of 64 °C and 1900 m^3/day. By contrast, at $k_f = 5 \times 10^{-13}$ m^2, the highest spring temperatures and discharges are obtained at *c*. 2000 years, while decreases of over 20 °C and 200 m^3/day occur at 10 000 years with respect to the peak temperature and flow rates respectively. In the latter case, the abrupt increase of the spring heat flux discharge is attributed to the onset of convective cells within the Lorusa Fault and in the adjoining step-over. After 2000 years, the convective cells continue to expand within the fault plane, bringing about a thermal perturbation relative to the surrounding country rock. However, the lateral migration of the convective flows results in a decrease of the heat flux discharges at springs. Assuming these conditions, the spring temperatures and discharges as modelled fulfill the calibration requirements of the Terme di Valdieri springs at *c*. 1500–1800 years. The isotherm distributions at 2500 and 10 000 years in the Lorusa Fault are shown in Figure 14, and Figure 15 provides a snapshot of the 3D spatial distribution of the 70 °C isotherm at 1500 years.

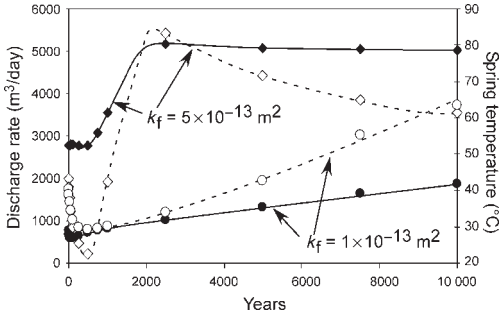

Fig. 13. Maximum flow rates and temperatures of waters discharging at springs v. years, plotted for fault permeabilities of 1×10^{-13} and 5×10^{-13} m^2 and host rock permeabilities of 1×10^{-15} m^2 using model 3. The BHF is 80 mW m^{-2}. Symbols (•) and (◆) represent water discharges, while (○) and (◇) represent maximum spring temperatures.

It is of interest to note that the thermal state of the jog region is highly perturbed, with a negative anomaly close to the Cougne Fault and a sharp positive anomaly close to the western end of the Lorusa Fault. The shape of this latter anomaly fits well with the field location of the Terme di Valdieri springs.

To check the consistency of this scenario, the sensitivity of the modelling results was checked against variations in the most uncertain assigned parameters by keeping $k_f = 5 \times 10^{-13}$ m^2 and $k_{hr} = 1 \times 10^{-15}$ m^2. Through these analyses, it was found that the effect of increasing the infiltration rates through the Lorusa Fault, the Cougne Fault and the step-over region more than three-fold (to 5×10^{-4} m/day) is reflected in a delay of 4000 years in the time interval at which the peak of spring temperatures and discharges occurs. Under this condition, the convective circulation is capable of beginning, providing results that are still consistent with those required by calibration. However, by further increasing the infiltration rate, the thermal convection is inhibited by advective circulation, and satisfactory results are never obtained in the 10 000 year time-range. Similarly, an analysis of the sensitivity of host rock porosity on the thermal system was performed, indicating that porosities of 0.01 instead of 0.1 cause a reduction of the simulated spring temperatures of at most 3 °C.

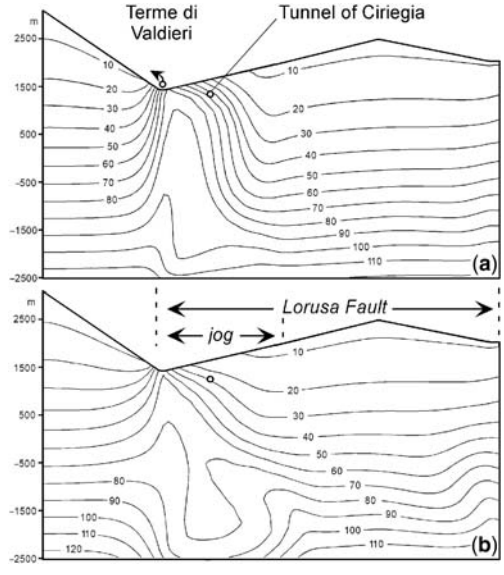

Fig. 14. Isotherm distribution across the Lorusa Fault obtained for $k_f = 5 \times 10^{-13}$ m^2 and $k_{hr} = 1 \times 10^{-15}$ m^2 using model 3. (**a**) Distribution after 2500 years and (**b**) after 10 000 years.

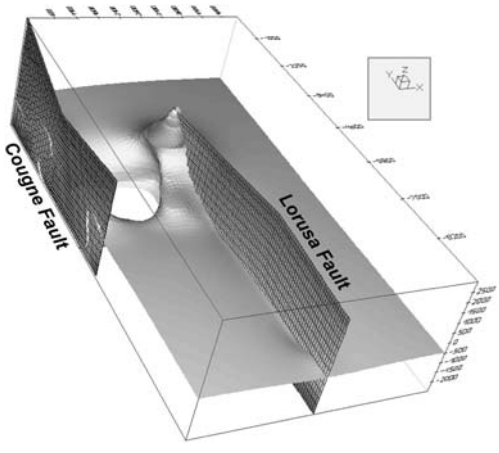

Fig. 15. Isosurface corresponding to a temperature of 70 °C (at $t = 1500$ years) visualized for a permeability of the Lorusa Fault, Cougne Fault, and jog of 5×10^{-13} m^2 and a host rock permeability of 1×10^{-15} m^2. Notice that, within the jog, a sharp transition occurs between a negative thermal anomaly located next to the Cougne Fault and a positive anomaly concentrated next to the Lorusa Fault. The latter is related to the upwelling and discharge of waters at the Terme di Valdieri springs.

Discussion

The simulations show that the type of structural configuration crucially affects the temporal variation of hot spring temperatures and discharges, in addition to the host rock and fault permeabilities. For the Terme di Valdieri flow system, a satisfactory fit between the numerical outputs and the measured spring temperatures of 70 °C and discharges of 50 kg s^{-1} is obtained only if the fault interaction scenario of model 3 is assumed. This scenario postulates that meteoric waters infiltrating through the Lorusa Fault and the Cougne Fault are transferred to the permeable jog structure where they finally upwell to the Valdieri springs. On the other hand, sensitivity tests carried out on fault and host rock permeabilities using model 1 and model 2 provided spring discharges and temperatures that are remarkably different than those required by the calibration specifications. Validation of model 3 was also possible both through increasing the recharge rate, one of the most unconstrained parameters, by up to three times (up to 200 mm a^{-1}) and by decreasing the porosity of host rocks by a factor of 10 (to 0.01).

By studying relationships between active hot springs and faults in a variety of tectonic settings, Curewitz & Karson (1997) have documented the common occurrence of hot springs in zones of fault interaction. In these zones, stress concentration promotes active fracturing and enhanced fluid flow despite clogging by hydrothermal mineral precipitates (Segall & Pollard 1980; Scholz & Anders 1994). For example, the strong localized enhancement of vertical permeability in a dilational jog is interpreted by Sibson (1987) to be the factor sustaining the powerful hydrothermal Salton Sea system of the southern San Andreas Fault. In the Argentera Massif, Perello *et al.* (2001) also proposed that the location of the thermal springs of Bagni di Vinadio (*c.* 17 km north of Valdieri) is attributable to the zone of enhanced fracturing that corresponds to a dilational step-over bounded by two NW-trending right-lateral faults. In this work, the numerical validation of a fault interaction model obtained through comparison of the different hypotheses provides a first quantitative constraint on the role played by jogs in controlling the location of thermal discharges. However, in the Terme di Valdieri sector, there is a lack of field and seismological evidence supporting the hypothesis that the contractional step-over bounded by the Lorusa and Cougne Faults represents a still-active structure with permeability dynamically maintained by fault propagation and active fracturing. Freshly exposed fracture surfaces in granite and the low salinity of fluids (Fancelli & Nuti 1978; Michard *et al.* 1989; Baietto 2007) suggest that clogging by hydrothermal minerals could not be efficient at filling fractures and at reducing permeability over relatively short periods (e.g., hundreds of years, Fournier 1991), as is indeed the case in many other geothermal settings (Elders *et al.* 1979; Sibson 1987). This circumstance could suggest that the Valdieri thermal flow system has not been affected by substantial decreases in permeability, even over thousands of years, and that the Lorusa and Cougne faults have been inactive during this period. Moreover, in this work, permeability within the jog was considered as isotropic and homogeneous across the whole region. Future numerical models applied in similar structural contexts should also take into account variations of fracture distribution and permeability gradients within the jog regions.

In the three model geometries considered, spring discharges with temperatures higher than ambient temperatures were produced by either advective or convective flows. However, the numerical results have shown that thermal convection is a requirement for providing water flow rates and temperatures such as those measured at the Terme di Valdieri springs. In a context like the Alps, thermal circulations have always been attributed to advective flows controlled by topographic gradients (Vuataz 1982; Rybach 1995; Perello 1997; Martinotti *et al.* 1999; Pastorelli *et al.* 1999, 2001; Perello *et al.* 2001). The results of this work

demonstrate that, provided permeabilities are adequate, thermal convection can develop in mountainous settings in combination with advective flows. Diagenetic processes, brine migration and ore deposition in many sedimentary basins (Prats 1966; Raffensperger & Vlassopoulos 1999; Garven *et al.* 2001; Thornton & Wilson 2007) and the upwelling of hot springs in the Basin and Range Province (López & Smith 1995) are some of the processes that are thought to be controlled by coexisting convective and advective flows (i.e., mixed convection).

In the Valdieri setting, convective circulations begin at fault permeabilities higher than 2×10^{-13} and 1×10^{-13} m^2 (at BHF values of 80 and 100 mW m^{-2} respectively) and at host rock permeabilities lower than 5×10^{-15} m^2. This permeability range is consistent with that indicated by López & Smith (1995) for the onset of convection in the Basin and Range province. However, the Valdieri simulations have also shown that the geometry of the flow system strongly influences the field where convection can occur. In fact, while this process activates in models 1 and 3 for the permeability ranges noted above, in model 2, convection in the Lorusa Fault is inhibited by the fluids downflowing from the S. Giovanni Fault. The effect of convection in the thermal system can be evaluated by comparing for all three models the cumulative heat (J) discharged at springs over 10 000 years, assuming $k_f = 5 \times 10^{-13}$ m^2 (Fig. 16). It can be seen that the difference in heat discharges in the three models increases over time. This reflects the onset of convective cells in models 1 and 3 (at *c*. 800 a) which results in an accelerated increase in heat discharge that does not occur in model 2. Moreover, this difference is also caused by the more vigorous convection occurring in model 3 with respect to model 1. At the Terme di Valdieri springs, the occurrence of granitic bodies located beneath migmatitic gneisses might represent an additional factor that can favor convective flows at shallow depths. In fact, the state of fracturing of the granites where large rock volumes are involved, as opposed to the fracturing within the migmatitic gneisses which is mostly concentrated along localized damage zones, creates the conditions for pervasive flows and focused flows, respectively. Thus, migmatitic gneisses sited above granites at the spring site, on the one hand can prevent massive infiltrations of cold meteoric waters (as would be expected in the case of outcropping granites), and on the other can promote the onset of thermal convective circulation within the granites. Similarly, in their thermohydraulic models in a mountainous setting, Forster & Smith (1988*a* & *b*) observed that a low-permeability layer was needed to allow thermal convection to occur without being suppressed by overlying topographically-driven flow.

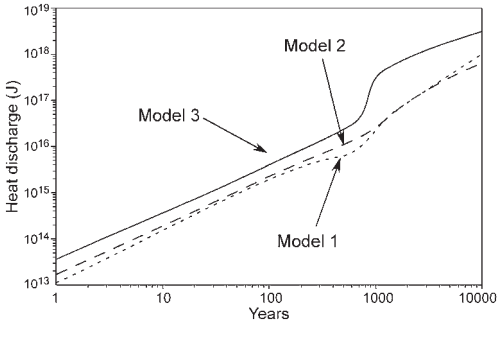

Fig. 16. Cumulative heat discharge at the Terme di Valdieri springs for the three models considered.

The fault interaction model (model 3) was validated by imposing a $k_f = 5 \times 10^{-13}$ m^2 to the Lorusa and Cougne Faults and to the jog inbetween. This remarkably high permeability with respect to the damage zones bounding the two faults falls within the range of permeability values obtained from laboratory tests (10^{-16}–10^{-11} m^2; Evans *et al.* 1997) and *in situ* tests (10^{-17}–10^{-11} m^2; Istok 1989; Phillips 1991; National Research Council 1996) of damage zones in faulted crystalline rocks in different geological settings. Moreover, the fault permeability values obtained by numerical modeling are consistent with the permeabilities obtained from slug tests that were performed in the St Anna borehole (Darcy 1997). This borehole, *c*. 1200 m deep, was drilled at *c*. 10 km to the NW of Valdieri in the Valletta Shear Zone, a NW-trending fault with hydraulic characteristics similar to those of the Lorusa and Cougne Faults. The tests indicated fault damage zone permeabilities greater than 10^{-14} m^2 (Baietto 2007).

With respect to host rock permeability, validation of model 3 was achieved through the adoption of a broad range of permeability values, in either the conductive or the advective field. This indicates that, for transient fluid and heat flows, the heat discharge at the springs is much more dependent on the fault than on the host rock permeability. However, it could be expected that the possible occurrence of pervasive flow around the fault zones could have important consequences for water–rock interaction and mineralization. If a large proportion of groundwater is directed towards the fault zone, the various chemical species brought into solution by water–rock interactions along the flow path will reach the fault zone, where they can promote processes such as hydrothermal alteration and mineral deposition.

In summary, simulation results show that thermal circulations in strike–slip fault systems can develop in contexts of single faults, of multiple faults linked at depth, or of faults connected by jogs. It might be useful to remember that, within the Alps, post-Oligocene tectonic activity led to the widespread development of these structural elements in both the internal and external portions of the mountain chain (Hubbard & Mancktelow 1992; Bistacchi & Massironi 2000; Tricart 2004; Giglia *et al.* 1996). However, the upwelling of hot springs and the occurrence of active thermal flow systems related to these features is much less commonly observed. Rough topography is a factor that promotes the infiltration of cold waters and the subsequent upwelling of waters with temperatures higher than ambient at valley bottoms (Forster & Smith 1988*a* & *b*; Jaboyedoff 1999; Pastorelli *et al.* 1999). However, the upwelling of thermal springs is often likely to be obliterated by low-permeability valley fills or by infiltration of cold waters from river beds. Numerical modelling of Valdieri reveals new constraints on this aspect, showing that permeable jogs sited at valley bottoms and hydraulically connected with strike–slip faults might represent a reasonable requirement for obtaining high spring temperatures and discharges. On the contrary, thermal systems that are controlled by single strike–slip faults or faults connected at depth could not be efficient enough to drive the upwelling of thermal springs.

One shortcoming of these models is the assumption, ignoring any information that could indicate the possible lifetime of the Terme di Valdieri flow system, of a steady-state solution as the initial condition for all transient-regime simulations. If this assumption were reasonable, the simulations show that the time required to attain the calibration conditions is *c*. 1500 years. In principle, this could ideally represent the period since the last seismic event caused an increase in fault and jog permeabilities through fracturing by fault displacement and stress concentration.

Conclusions

Comparison of the numerical solutions obtained for thermal circulation scenarios using a single fault, faults intersecting at depth and faults interacting through a permeable jog have provided a better understanding of the influence exerted by these structures. This applies both to the bulk fluid and heat patterns within geothermal systems and to the temporal variations of heat discharge at springs. A satisfactory calibration of the numerical results with the measured temperature of 70 °C and discharges of 50 kg s^{-1} was obtained by assuming a fault jog interaction context. In this framework, the thermal discharges at Terme di Valdieri can be seen to be controlled by circulations that occur both in the Lorusa Fault and in the Cougne Fault, that interact by means of a permeable step-over located at the bottom of the valley. Simulations of circulation in a single fault (i.e., the Lorusa Fault) and in faults that intersect at depth (i.e., the Lorusa and San Giovanni Fault) provided heat discharges that are not nearly as high as those provided by a jog context. The reason for this is that the enhanced permeability in the jog region favours the onset of vigorous convective circulations. Once the onset occurs, the spring temperatures and flow rates of springs increase rapidly, attaining the values required by the model calibration at *c*. 1500 years under the assumption of a initial steady-state flow condition. After this period, owing to the lateral expansion of the convective cells within the fault plane, the heat flux discharge slightly decreases. Thermal convection can also develop within single faults, but it seems to be less efficient in drawing high heat fluxes into springs than convection developed in jog and fault contexts. This finding demonstrates that thermal convection is a viable process that can occur in strike–slip fault systems within basement that can also coexist with advective flows in mountainous regions. Assuming for the geological setting of Valdieri a basal heat flow of 80 mW m^{-2}, the requirements for the development of convection are a fault permeability higher than 2×10^{-13} m^2, a host rock permeability lower than 5×10^{-15} m^2, and infiltration rates lower than 200 mm a^{-1}. If higher values of basal heat flow are assumed, the convective region expands in permeability space. Moreover, under these conditions, convection within the fault and the jog can develop in cases where heat transfer in the host rock is predominantly of either conductive or advective type, that is, for host rock permeabilities lower or higher than 3×10^{-17} m^2, respectively. By contrast, simulations of thermal flows occurring in faults that intercept at depth have shown that the development of thermal convection in this setting is inhibited by advective perturbation at the base of faults. In this setting, the cumulative heat flux discharged at springs is remarkably lower than that produced in the other contexts. Finally, the use of numerical modelling for comparing spring response under different structural configurations provides a first quantitative estimate of the importance of jog structures in controlling the localization of thermal discharges in strike–slip fault systems. This finding opens up new perspectives in the field of geothermal exploration, particularly considering the currently increased interest in renewable sources of energy. It must be emphasized that, despite large

uncertainties in the factors that can exert substantial control on the water circulation within geothermal systems, numerical modelling can be appropriately used with some degree of confidence as a tool for checking the consistency of structural hypotheses.

We are grateful to J. Imber and R. Holdsworth for the constructive review, which helped to improve the quality of the manuscript. The Centre d'Hydrogéologie de l'Université de Neuchâtel (CHYN) is acknowledged for the use of the Feflow package. This research has been financially supported by Italian MIUR (Ministero dell'Istruzione, dell'Università e della Ricerca), grants awarded to P. Cadoppi.

References

ALFÖLDI, L., GÁLFI, J. & LIEBE, P. 1985. Heat flow anomalies caused by water circulation, *Journal of Geodynamics*, **4**, 199–217.

BAIETTO, A. 2007. *Fault-related thermal circulations in the Argentera Massif (south-western Alps)*. PhD thesis, Earth Science Department, University of Turin.

BARTON, C. A., ZOBACK, M. D. & MOOS, D. 1995. Fluid flow along potentially active faults in crystalline rocks. *Geology*, **23**, 683–686.

BENOIT, W. R. 1999. Conceptual models of the Dixie Valley, Nevada, geothermal system. *Geothermal Resources Council Transactions*, **23**, 505–511.

BETHKE, C. M. & MARSHAK, S. 1990. Brine migrations across North America – the plate tectonics of groundwater. *Annual Reviews of Earth and Planetary Sciences*, **18**, 287–315.

BIGOT-CORMIER, F., POUPEAU, G. & SOSSON, M. 2000. Dénudation différentielles du massif cristallin externe alpin de l'Argentera (Sud-Est de la France) révélées par thermochronologie traces de fission (apatites, zircons). *Comptes Rendus del' Academie des Sciences de Paris, Earth and Planetary Sciences*, **330**, 363–370.

BIRD, R. B., STEWART, W. E. & LIGHTFOOT, E. N. 1960. *Transport Phenomena*, Wiley, New York.

BISTACCHI, A. & MASSIRONI, M. 2000. Post-nappe brittle tectonics and kinematic evolution of the northwestern Alps: an integrated approach. *Tectonophysics*, **327**, 267–292.

BOGDANOFF, S. 1986. Evolution de la partie occidentale du Massif cristallin externe de l'Argentera. Place dans l'arc Alpin. *Géologie de France*, **4**, 433–453.

BORTOLAMI, G. & GRASSO, F. 1969. Osservazioni geologico-applicative sul cunicolo d'assaggio del traforo del Ciriegia e considerazioni sull'intero tracciato. *Procedures of I International Congress: 'Problemi tecnici nella costruzione di gallerie'*, 111–126.

BRACE, W. F., PAULDING, B. W. & SCHOLZ, C. H. 1966. Dilatancy in the fracture of crystalline rocks. *Journal Geophysical Resources*, **71**, 3939–3953.

BREDEHOEFT, J. D. & HANSHAW, B. B. 1968. On the maintenance of anomalous fluid pressures; 1, thick sedimentary sequences. *GSA Bulletin*, **79**, 1097–1106.

CAINE, J. S., EVANS, J. P. & FORSTER, C. B. 1996. Fault zone architecture and permeability structure. *Geology*, **24**, 1025–1028.

CALAIS, E., GALISSON, L. *ET AL*. 2000. Crustal strain in the Southern Alps, France, 1948–2000. *Tectonophysics*, **319**, 1–17.

CHAPMAN, D. S. & FURLONG, K. P. 1992. Thermal state of the continental crust. *In*: FOUNTAIN, D. M., ARCULUS, R. J. & KAY, R. W. (eds) *Continental Lower Crust: Developments in Geotectonics.* Elsevier, Amsterdam, **23**, 179–199.

COX, S. F., KNACKSTEDT, M. A. & BRAUN, J. 2001. Principles of structural control on permeability and fluid flow in hydrothermal systems. *Reviews in Economic Geology*, **14**, 1–24.

COURBOULEX, F., DESCHAMPS, A. *ET AL*. 1998. Source study and tectonic implications of the Ventimiglia (border of Italy and France) earthquake (M_L= 4.7). *Tectonophyisics*, **290**, 245–257.

CUREWITZ, D. & KARSON, J. 1997. Structural settings of hydrothermal outflow: fracture permeability maintained by fault propagation and interaction. *Journal of Volcanology and Geothermal Research*, **79**, 149–168.

CUTILLO, P. A., SCREATON, E. J. & GE, S. 2003. Three-dimensional numerical simulation of fluid flow and heat transport within the Barbados Ridge accretionary complex. *Journal of Geophysical Research*, **108**, 2555, doi:10.1029/2002JB002240.

DARCY, J. 1997. La nouvelle liaison routiere Nice-Cuneo et le Tunnel du Mercantour. *Tunnels et ouvrages souterrains*, **139**, 46–50.

DIERSCH, H.-J. G. 1998. *FeFlow® – Finite Element Subsurface Flow & Transport Simulation System.* Wasy Software GmbH.

ELDERS, W. A., HOAGLAND, J. R., MCDOWELL, S. D. & COBO, J. M. 1979. Hydrothermal mineral zones in the geothermal reservoir of Cerro Prieto. *Geothermics*, **8**, 201–209.

EVANS, D. G. & RAFFENSPERGER, J. P. 1992. On the stream function for variable-density groundwater flow. *Water Resources Research*, **28**, 2141–2145.

EVANS, J. P., FORSTER, C. B. & GODDARD, J. V. 1997. Permeability of fault-related rocks, and implications for hydraulic structure of fault zones. *Journal of Structural Geology*, **19**, 11, 1393–1404.

FANCELLI, R. & NUTI, S. 1978. Studio geochimico delle sorgenti termali del Massiccio Cristallino dell'Argentera (Alpi Marittime). *Boll. Soc. Geol. It.*, **97**, 115–130.

FAULKNER, D. R. & RUTTER, E. H. 2001. Can the maintenance of overpressured fluids in large strike–slip fault zones explain their apparent weakness? *Geology*, **29**, 503–506.

FAURE-MURET, A. 1955. Etudes géologiques sur le massif de l'Argentera. *In*: BOILLOT, G. (ed.) *Les Marges continentales actuelles et fossiles autour de la Mercantour et ses enveloppes sédimentaires*. Mémoires pour servir à l'explication de la carte géologique détaillé de la France. Imprimerie Nationale, Paris.

FEHN, U. & CATHLES, L. 1979. Hydrothermal convection at slow-spreading midocean ridges. *Tectonophysics*, **55**, 239–260.

FORSTER, C. & SMITH, L. 1988*a*. Groundwater flow systems in mountainous terrain, 1, numerical modelling technique. *Water Resources Research*, **24**, 999–1010.

FORSTER, C. & SMITH, L. 1988*b*. Groundwater flow systems in mountainous terrain, 2, controlling factors. *Water Resources Research*, **24**, 1011–1023.

FORSTER, C. & SMITH, L. 1989. The influence of groundwater flow on thermal regimes in mountainous terrain: a model study. *Journal of Geophysical Research*, **85**, 1867–1875.

FOURNIER, R. O. 1991. The transition from hydrostatic to greater than hydrostatic fluid pressure in active hydrothermal systems in crystalline rocks. *Geophysical Research Letters*, **18**, 955–958.

FRY, N. 1989. Southwestward thrusting and tectonics of the western Alps. *In*: COWARD, M., DIETRICH, D. & PARK, R. G. (eds) *Alpine Tectonics*. Geological Society, London, Special Publications, **45**, 83–111.

GARVEN, G., GE, S., PERSON, M. A. & SVERJENSKY, D. A. 1993. Genesis of stratabound ore deposits in the midcontinent basins of North America, 1, The role of regional groundwater flow. *American Journal of Science*, **293**, 497–568.

GARVEN, G., BULL, S. W. & LARGE, R. R. 2001. Hydrothermal fluid flow models of stratiform ore genesis in the McArthur Basin, Northern Territory, Australia. *Geofluids*, **1**, 289–311.

GHAFIRI, A. 1995. *Paléosismicité de failles actives en contexte de sismicité modérée: application à l'évaluation de l'aléa sismique dans le Sud-Est de la France*. PhD thesis, Univ. Paris XI.

GIGLIA, G., CAPPONI, G., CRISPINI, L. & PIAZZA, M. 1996. Dynamics and seismotectonics of the West-Alpine arc. *Tectonophysics*, **267**, 143–175.

GRATIER, J. P., FAVREAU, P. & RENARD, F. 2003. Modeling fluid transfer along California faults when integrating pressure solution crack sealing and compaction processes. *Journal of Geophysical Research*, **108**, 2104, doi:10.1029/2001JB000380.

HENLEY, R. W. & ADAMS, D. P. M. 1992. Strike–slip fault reactivation as a control on epithermal vein-style gold mineralization. *Geology*, **20**, 443–446.

HENRY, P. 2000. Fluid flow at the toe of the Barbados accretionary wedge constrained by thermal, chemical and hydrogeologic observations and models. *Journal of Geophysical Research*, **105**, 25855–25872.

HICKMAN, S., SIBSON, H. R. & BRHUN, R. 1995. Introduction to special section: mechanical involvement of fluids in faulting. *Journal of Geophysical Research*, **100**, B7, 12.831–12.840.

HUBBARD, M. & MANCKTELOW, N. S. 1992. Lateral displacement during Neogene convergence in the western and central Alps. *Geology*, **20**, 943–946.

INGEBRITSEN, S. E. & MANNING, C. E. 1999. Geological implications of a permeability–depth curve for the continental crust. *Geology*, **27**, 1107–1110.

ISTOK, J. 1989. *Groundwater Modelling by Finite Element Method*, Vol. 13. American Geophysical Union, Water Resources Monograph, Washington, DC.

JABOYEDOFF, M. 1999. Modèles thermiques simples de la croûte terrestre: un regard sur les Alpes. *Bullettin de la Société Vaudoise des Sciences Naturelles*, **86**, 229–271.

JABOYEDOFF, M. & PASTORELLI, S. 2003. Perturbation of the heat flow by water circulation in a mountainous framework. Examples from the Swiss Alps. *Eclogae Geologicae Helvetiae*, **96**, 37–47.

KASAMEYER, P., YOUNKER, L. & HANSON, J. 1984. Development and application of a hydrothermal model for the Salton Sea Geothermal Field, California. *Bulletin of the Geological Society of America*, **95**, 1242–1252.

LARROQUE, C., BÉTHOUX, N. *ET AL*. 2001. Active and recent deformation at the Southern Alps–Ligurian basin junction. *Geologie en Mijnbouw*, **80**, 255–272.

LÓPEZ, D. L. & SMITH, L. 1995. Fluid flow in fault zones: Analysis of the interplay of convective circulation and topographically driven groundwater flow. *Water Resources Research*, **31**, 1489–1503.

LÓPEZ, D. L. & SMITH, L. 1996. Fluid flow in fault zones: influence of hydraulic anisotropy and heterogeneity on the fluid flow and heat transfer regime. *Water Resources Research*, **32**, 3227–3235.

MALARODA, R., CARRARO, F., DAL PIAZ, G. V., FRANCESCHETTI, B., STURANI, C. & ZANELLA, E. 1970. Carta geologica del Massiccio dell'Argentera alla scala 1:50 000 e note illustrative. *Memoire della Società Geologica Italiana*, **9**, 557–663.

MANNING, C. E. & INGEBRITSEN, S. E. 1999. Permeability of the continental crust: implications of geothermal data and metamorphic systems. *Reviews of Geophysics*, **37**, 127–150.

MARINI, L., BONARIA, V., GUIDI, M., HUNZIKER, J. C., OTTONELLO, G. & VETUSCHI ZUCCOLINI, M. 2000. Fluid geochemistry of the Acqui Terme–Visone geothermal area (Piemonte, Italy). *Applied Geochemistry* **15**, 917–935.

MARTINOTTI, G., MARINI, L., HUNZIKER, J. C., PERELLO, P. & PASTORELLI, S. 1999. Geochemical and geothermal study of springs in the Ossola-Simplon Region. *Eclogae Geologicae Helvetiae*, **92**, 295–305.

MCKENNA, J. R. & BLACKWELL, D. D. 2004. Numerical modelling of transient Basin and Range extensional geothermal systems. *Geothermics*, **33**, 457–476.

MERCER, J. W. & PINDER, G. F. 1974. *Finite Element Analysis of Hydrothermal Systems, Finite Element Methods in Flow Problems*. University of Alabama Press, Tuscaloosa, AL.

MICHARD, G., GRIMAUD, D., D'AMORE, F. & FANCELLI, R. 1989. Influence of mobile ion concentrations on the chemical composition of geothermal waters in granitic areas, example of hot springs from Piemonte (Italy). *Geothermics*, **18**, 729–741.

National Research Council 1996. *Rock Fractures and Fluid Flow*. Washington, DC.

NEUZIL, C. E. 1995. Abnormal pressures as hydrodynamic phenomena. *American Journal of Science*, **295**, 742–786.

PARRY, W. T. 1998. Fault-fluid compositions from fluid inclusion observations and solubilities of fracture-sealing minerals. *Tectonophysics*, **290**, 1–26.

PASTORELLI, S., MARINI, L. & HUNZIKER, J. C. 1999. Water chemistry and isotope composition of the Acquarossa thermal system, Ticino, Switzerland. *Geothermics*, **28**, 75–93.

PASTORELLI, S., MARINI, L. & HUNZIKER, J. C. 2001. Chemistry, isotope values (δD, δ^{18}O, $\delta^{34}S_{SO4}$) and temperatures of the water inflows in two Gotthard tunnels, Swiss Alps. *Applied Geochemistry*, **16**, 633–649.

PERELLO, P. 1997. *Interazioni tra strutture tettoniche, fenomeni di sollevamento rapido recente e emanifestazioni*

geotermiche a bassa entalpia nelle Alpi occidentali. Studio di quattro località tipo: Settore Ossolano, Alta Valle d'Aosta, Settore Vallesano, Massiccio dell'Argentera. PhD thesis, Earth Science Department, University of Turin, Italy.

PERELLO, P., MARINI, L., MARTINOTTI, G. & HUNZIKER, J. C. 2001. The thermal circuits of the Argentera Massif (western Alps, Italy): an example of low-enthalpy geothermal resources controlled by Neogene alpine tectonics. *Eclogae Geologicae Helvetiae*, **94**, 75–94.

PERROCHET, P. & TACHER, L. 1997. *Mathematical modeling of hydro-thermal processes in Mururoa Atoll*. Research Report GEOLEP-EPFLDGC, University of Lausanne.

PHILLIPS, O. M. 1991. *Flow and Reactions in Permeable Rocks*. Cambridge University Press, New York.

PRATS, M. 1966. The effect of horizontal fluid flow on thermally induced convection currents in porous mediums. *Journal of Geophysical Research*, **71**, 4835–4837.

RAFFENSPERGER, J. & VLASSOPOULOS, D. 1999. The potential for free and mixed convection in sedimentary basins. *Hydrogeology Journal*, **7**, 505–520.

RITZ, J-F. 1991. *Evolution du champ de contrainte dans les Alpes du Sud depuis la fin de l'Oligocène, implications sismotectoniques*. PhD thesis, Université Montpellier II.

RYBACH, L. 1981. Geothermal systems, conductive heat flow, geothermal anomalies. *In*: RYBACH, L. & MUFLLER, L. J. P. (eds) *Geothermal Systems*. Wiley, New York, 3–36.

RYBACH, L. 1995. Thermal waters in deep Alpine tunnels. *Geothermics*, **24**, 631–637.

SCHOLZ, C. H. & ANDERS, M. H. 1994. The permeability of faults. *In*: HICKMAN, S. H., SIBSON, R. H. & BRUHN, R. (eds) *Proceedings of Workshop LXIII on the Mechanical Involvement of Fluids in Faulting*. USGS Open file report, **94–228**, 247–253.

SEGALL, P. & POLLARD, D. D. 1980. Mechanics of discontinuous faults. *Journal of Geophysical Research*, **85**, 4337–4350.

SIBSON, R. H. 1987. Earthquake rupturing as a mineralizing agent in hydrothermal systems. *Geology*, **15**, 701–704.

SIBSON, R. H. 1994. Crustal stress, faulting and fluid flow. *In*: PARNELL, J. (ed.) *Geofluids: Origin, Migration and Evolution of Fluids in Sedimentary Basins*. Geological Society, London, Special Publications, **78**, 69–84.

SIBSON, R. H. 2001. Seismogenic framework for hydrothermal transport and ore deposition. Structural controls on ore genesis. *Reviews in Economic Geology*, **14**, 25–50.

SIBSON, R. H. & SCOTT, J. 1998. Stress/fault controls on the containment and release of overpressured fluids: examples from gold-quartz vein systems in Juneau, Alaska, Victoria, Australia, and Otago, New Zealand. *Ore Geology Reviews*, **13**, 293–306.

SIMMS, M. A. & GARVEN, G. 2004. Thermal convection in faulted extensional sedimentary basins: theoretical results from finite-element modelling. *Geofluids*, **4**, 109–130.

SMITH, D. A. 1980. Sealing and nonsealing faults in Louisiana Gulf Coast salt basin. *American Association of Petroleum Geologists Bulletin*, **64**, 145–172.

THORNTON, M. M. & WILSON, A. M. 2007. Topography-driven flow versus buoyancy-driven flow in the U. S. mid-continent: implications for the residence time of brines. *Geofluids*, **7**, 69–78.

TRAVIS, B. J., JANECKY, D. R. & ROSENBERG, N. D. 1991. Three-dimensional simulation of hydrothermal circulation at mid-ocean ridges. *Geophysical Research Letters*, **18**, 1441–1444.

TRICART, P. 2004. From extension to transpression during the final exhumation of the Pelvoux and Argentera massifs, Western Alps. *Eclogae Geologicae Helvetiae*, **97**, 429–439.

VUATAZ, F.-D. 1982. *Hydrogéologie, géochimie et géothermie des eaux thermals de Suisse et des regions alpines limitrophes*. Matériaux pour la Géologie de la Suisse, Série Hydrologie, **29**, Kümmerly & Frey, Berne.

WISIAN, K. W. & BLACKWELL, D. D. 2004. Numerical modelling of Basin and Range geothermal systems. *Geothermics*, **33**, 713–741.

WOODCOCK, N. H. & FISCHER, M. 1986. Strike–slip duplexes. *Journal of Structural Geology*, **8**, 725–735.

YEAMANS, F. 1983. *Basin and Range Geothermal Hydrology: an Empirical Approach*. Special Report. Geothermal Resources Council, **13**, 159–174.